Research Paper

GEOSPHERE

GEOSPHERE

https://doi.org/10.1130/GES02514.1

14 figures; 1 set of supplemental files

CORRESPONDENCE: steve.rowland@unlv.edu

CITATION: Rowland, S.M., Korolev, S., Hagadorn, J.W., and Ghosh, K., 2023, Frenchman Mountain Dolostone: A new formation of the Cambrian Tonto Group, Grand Canyon and Basin and Range, USA: Geosphere, https://doi.org/10.1130/GES02514.1.

Science Editor: David E. Fastovsky
Associate Editor: Gregory D. Hoke

Received 15 January 2022
Revision received 14 October 2022
Accepted 23 November 2022

Published online 23 March 2023

Frenchman Mountain Dolostone: A new formation of the Cambrian Tonto Group, Grand Canyon and Basin and Range, USA

Stephen M. Rowland[1,2], Slava Korolev[1], James W. Hagadorn[3], and Kaushik Ghosh[4]

[1]Department of Geoscience, University of Nevada Las Vegas, Las Vegas, Nevada 89154, USA
[2]Las Vegas Natural History Museum, Las Vegas, Nevada 89101, USA
[3]Department of Earth Sciences, Denver Museum of Nature and Science, 2001 Colorado Boulevard, Denver, Colorado 80238, USA
[4]Department of Mathematical Sciences, University of Nevada Las Vegas, Las Vegas, Nevada 89154, USA

ABSTRACT

We describe, interpret, and establish a stratotype for the Frenchman Mountain Dolostone (FMD), a new Cambrian stratigraphic unit that records key global geochemical and climate signals and is well exposed throughout the Grand Canyon and central Basin and Range, USA. This flat-topped carbonate platform deposit is the uppermost unit of the Tonto Group, replacing the informally named "undifferentiated dolomites." The unit records two global chemostratigraphic events—the Drumian Carbon Isotope Excursion (DICE), when $\delta^{13}C_{carb}$ (refers to "marine carbonate rocks") values in the FMD dropped to –2.7‰, and the Steptoean Positive Carbon Isotope Excursion (SPICE), when the values rose to +3.5‰. The formation consists of eight lithofacies deposited in shallow subtidal to peritidal paleoenvironments. At its stratotype at Frenchman Mountain, Nevada, the FMD is 371 m thick. Integration of regional trilobite biostratigraphy and geochronology with new stratigraphy and sedimentology of the FMD, together with new $\delta^{13}C_{carb}$ chemostratigraphy for the entire Cambrian succession at Frenchman Mountain, illustrates that the FMD spans ~7.2 m.y., from Miaolingian (lower Drumian, *Bolaspidella* Zone) to Furongian (Paibian, *Dicanthopyge* Zone) time. To the west, the unit correlates with most of the Banded Mountain Member of the ~1100-m-thick Bonanza King Formation. To the east, at Grand Canyon's Palisades of the Desert, the FMD thins to 8 m due to pre–Middle Devonian erosion that cut progressively deeper cratonward. Portions of the FMD display visually striking, meter-scale couplets of alternating dark- and light-colored peritidal facies, while other portions consist of thick intervals of a single peritidal or shallow subtidal facies. Statistical analysis of the succession of strata in the stratotype section, involving Markov order and runs order analyses, yields no evidence of cyclicity or other forms of order. Autocyclic processes provide the simplest mechanism to have generated the succession of facies observed in the FMD.

INTRODUCTION

The Tonto Group of the southwestern U.S. has played a key role in the understanding of Cambrian Earth history for over a century. It traditionally consists of three formations that were originally defined in the central portion of the Grand Canyon—the Tapeats Sandstone, Bright Angel Shale, and Muav Limestone (Fig. 1; Gilbert, 1875; Powell, 1876; Noble, 1914, 1922). The names of the upper two of these units have recently been modified to reflect the heterogeneity of their lithologies (Bright Angel Formation and Muav Formation; Karlstrom et al., 2020), and two "new" rock formations have been added to the succession. At the base of the Tonto Group is the uppermost Sixtymile Formation, a heterolithic unit that conformably underlies the Tapeats Sandstone (Karlstrom et al., 2018, 2020). At the top of the Tonto Group is the oft-overlooked and previously temporally unconstrained Frenchman Mountain Dolostone (FMD), which is the subject of this paper.

The FMD has been challenging to decipher for multiple reasons: (1) its cliff-forming exposures are difficult to reach, (2) it has not yet yielded datable fossils, (3) its upper and lower contacts manifest themselves differently across the basin, and (4) its thickness varies greatly across a large geographic region. These characteristics made it difficult to confidently map and study by early stratigraphers in the Grand Canyon region. Noble (1922) distinguished this succession of dolostones as "subdivision A" of the Muav Limestone (Fig. 2A). Schenk and Wheeler (1942) lumped Noble's "subdivision 'A'" dolostones with the upper portions of the Muav as "Cambrian(?) and post-Cambrian limestones and dolomites" (Fig. 2A). McKee (1945) then divided the Muav Limestone into seven members, but he did not include Noble's (1922) "subdivision A;" he referred to that interval simply as "Cambrian undifferentiated dolomites" (Fig. 2A). This dolomitic interval, which ranges in thickness from just a few meters in eastern Grand Canyon to 371 m at Frenchman Mountain near Las Vegas, Nevada, has been ignored in most subsequent treatments of Grand Canyon stratigraphy. It has yielded no datable fossils, so its precise age has long been unknown. In stratigraphic columns that include the Tonto Group, McKee's "undifferentiated dolomites" are commonly included with the Muav Formation (e.g., Beus and Morales, 2003; Blakey and Middleton, 2012).

Brathovde (1986) examined the sedimentology and stratigraphy of this unnamed unit, primarily in Grand Canyon exposures. He searched

Stephen Rowland https://orcid.org/0000-0003-4800-7802

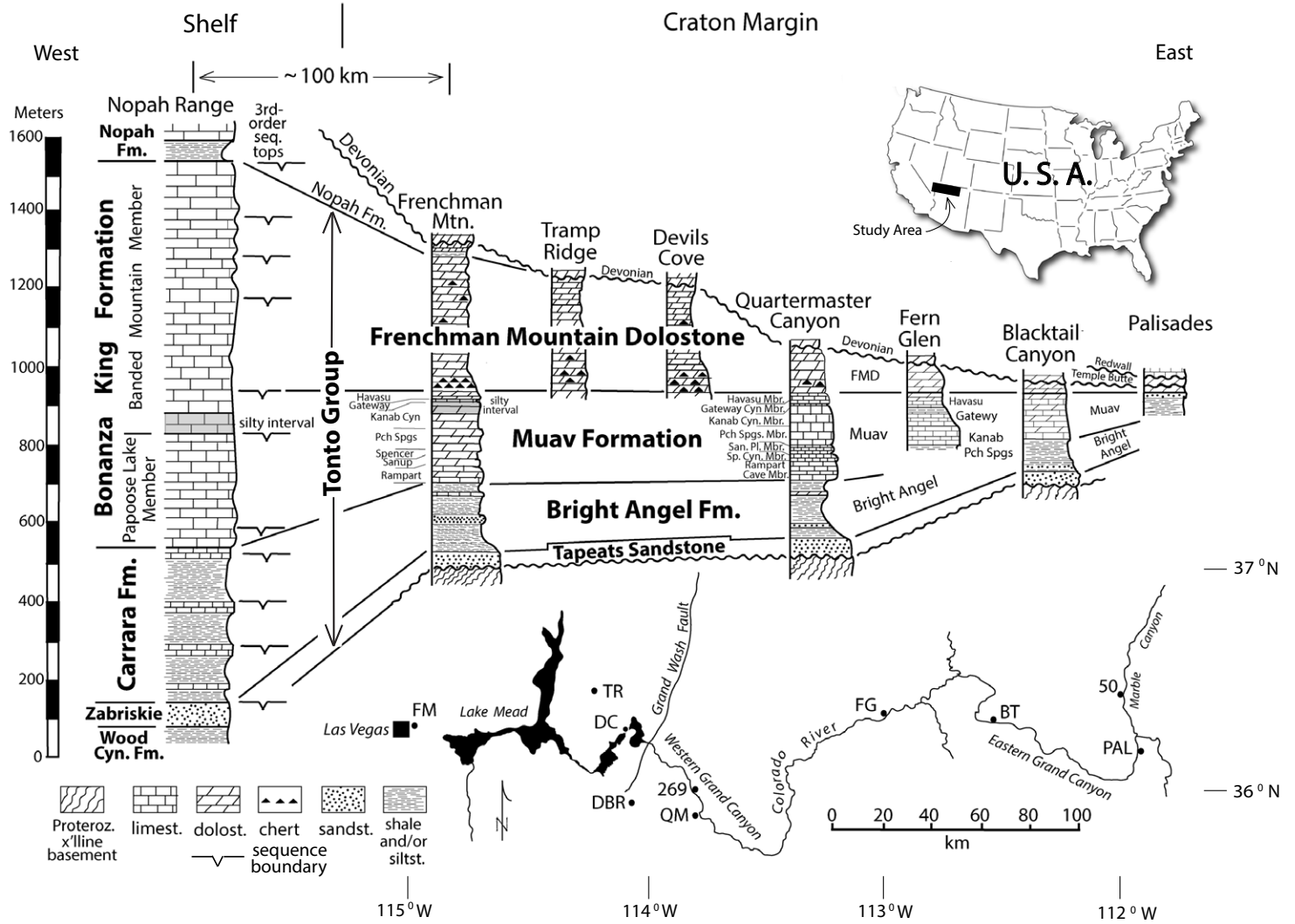

Figure 1. Index map and generalized stratigraphic columns and weathering profiles of Cambrian strata, from shelf exposures (Nopah Range, California, USA) to craton margin exposures (Frenchman Mountain, Nevada, and Grand Canyon, Arizona), showing thicknesses and correlations. The right four columns are in the Colorado Plateau geologic province; the left four columns are in the Basin and Range province. The 100 km distance between Frenchman Mountain and the Nopah Range is the present distance, not the pre-Neogene-extension distance, which was much less. Nopah Range data are from Keller et al. (2012). Sub–Frenchman Mountain Dolostone (FMD) thicknesses and lithologies at Quartermaster Canyon (Arizona) are from McKee (1945), although McKee identified "tongues of Bright Angel" directly above the Rampart Cave, Sanup Plateau (San. Pl.), and Spencer Canyon (Sp. Cyn.) (all in Arizona) Members of the Muav Formation; we include those intervals with the underlying Muav members. Fern Glen Canyon (Arizona) data are from Rowland et al. (1995). Data from Blacktail Canyon (Arizona) are from Rose (2003, 2011). Palisades of the Desert (Arizona) data are new, collected in 2019. All other data are from Korolev (1997). FM—Frenchman Mountain, Nevada; TR—Tramp Ridge, Nevada; DC—Devils Cove, Nevada; DBR—Diamond Bar Ranch, Arizona; 269—269-Mile canyon, Arizona; QM—Quartermaster Canyon, Arizona; FG—Fern Glen Canyon, Arizona; BT—Blacktail Canyon, Arizona; PAL—Palisades of the Desert, Arizona; 50—50-Mile creek, Arizona. Pch Spgs–Peach Springs; Cyn.–Canyon.

A. Grand Canyon exposures

Gilbert, 1975	Noble, 1922		Schenk and Wheeler, 1942	McKee, 1945	Brathovde, 1986	Korolev, 1997	Karlstrom et al., 2020	This study
Marbled Limestone	Muav Limestone	Subdivision A	Cambrian (?) and post-Cambrian limestones and dolomites	undifferentiated dolomites	Grand Wash Dolomite	Frenchman Mountain Dolomite	Frenchman Mountain Dolostone	Frenchman Mountain Dolostone
		Subdivisions B, C, D	Mead Limestone	Muav Limestone (with 7 named members)	Muav Limestone	Muav Limestone	Muav Formation	Muav Formation
			Peasley Limestone					

B. Southern Nevada cratonal exposures

Longwell et al., 1965	Gans, 1974	Matti et al., 1993	Montañez & Osleger, 1993; Osleger & Montañez, 1996	Korolev, 1997	Castor et al., 2000	Page et al., 2004	Karlstrom et al., 2020	This study
Bonanza King Formation				Frenchman Mountain Dolomite		Bonanza King Formation	Frenchman Mountain Dolostone	
				Muav Limestone			Muav Formation	

Figure 2. History of stratigraphic nomenclature applied to the Muav Formation and overlying dolostones.

unsuccessfully for conodonts and other biostratigraphically useful fossils and was therefore unable to constrain the age of this interval. He proposed that the unit be named the "Grand Wash Dolomite." That name was never published in the peer-reviewed literature, however, and Elston (1989) indicated that it violated the North American Stratigraphic Code because the name "Grand Wash" was already in use for a different stratigraphic unit in the same area—the Grand Wash Basalt. Korolev (1997), using a sequence-stratigraphic approach, extended the analysis of this unit westward to the thick exposure at Frenchman Mountain, where these supra-Muav dolostones are overlain by the sparsely fossiliferous but well-dated Furongian Nopah Formation (Miller et al., 1981). That section thus constrained, for the first time, the age of McKee's undifferentiated dolomites to Cambrian Series 3 (Miaolingian), except for the uppermost portion, as discussed below. Korolev (1997) proposed the name Frenchman Mountain Dolomite, which has subsequently been used on two geologic maps (Castor et al., 2000; Garside et al., 2012), a stratigraphic note (Rowland and Korolev, 2011), and—in the slightly modified form, Frenchman Mountain Dolostone—in a journal article (Karlstrom et al., 2020) and a published field guide (Rowland, 2022). However, this name is not yet in compliance with the North American Stratigraphic Code (North American Commission on Stratigraphic Nomenclature, 2005) because a detailed description of the strata has not been published in a recognized scientific medium and no stratotype section has been formally established. We fulfill those criteria with this paper.

Frenchman Mountain is a regionally important exposure, not only of the eponymous Frenchman Mountain Dolostone (FMD) described here, but for the Tonto Group as a whole. At Frenchman Mountain, the complete succession is readily accessible and extremely well exposed. The section dips ~50° to the east, and the Tonto Group here displays a thickness transitional (~860 m) between that of cratonal sections of the Tonto Group in the eastern Grand Canyon (~250 m) and of shelf sections of correlative strata in the southern Great Basin region (~1500 m). Hence, the Frenchman Mountain exposure helps to constrain the position of the hingeline of the Cambrian shelf. It is within the upper plate of a west-translated Miocene detachment fault that restores ~60 km to the east to a position near Gold Butte, Nevada (Longwell, 1974; Fryxell and Deubendorfer, 2005), within a few tens of kilometers of Grand Wash Cliffs sections in Arizona examined by Brathovde (1986) and McKee (1945). The inclusion of the FMD in the Tonto Group, together with the recognition of the presence of the Tonto Group at Frenchman Mountain, is thus stratigraphically appropriate, and it establishes a valuable link between Grand Canyon Cambrian sections and sections in the southern Great Basin.

Because Frenchman Mountain lies within the Basin and Range province, adjacent to the southern Great Basin, the first generation of stratigraphic terminology applied to this section was Great Basin terminology (Longwell et al., 1965; Gans, 1974)—a tradition that some workers continued into the 1990s and beyond (Matti et al., 1993; Montañez and Osleger, 1993; Osleger and Montañez, 1996; Osleger et al., 1996; Webster, 2011b). Thus, the strata that we refer to the FMD and Muav Formation in this paper were formerly considered to be portions of the Bonanza King Formation (Fig. 2), whereas the strata we refer to the Bright Angel Formation were originally assigned to the Pioche Shale, Lyndon

Limestone, and Chisholm Shale. The transition from southern Great Basin terminology to Colorado Plateau terminology, beginning in 1990 (Rowland et al., 1990; Castor et al., 2000), was driven by the growing recognition that Frenchman Mountain is fundamentally a cratonal section with palinspastic proximity to the Colorado Plateau.

The FMD was deposited in equatorial latitudes on the north-facing margin of Laurentia. The continent was oriented ~90° clockwise in comparison with its present orientation (Rowland and Shapiro, 2002; Torsvik and Cocks, 2017). Seaward of the craton-margin region where the FMD was being deposited was the "Great American Carbonate Bank" (Fritz et al., 2012; Taylor et al., 2012), the most extensive carbonate platform accumulation on Earth at that time (Kiessling et al., 2003).

The purposes of this paper are to (1) formally name the Frenchman Mountain Dolostone, (2) establish its age and regional stratigraphic relationships, and (3) describe and interpret the sedimentology, chemostratigraphy, and regional biostratigraphic framework of this unit, with an emphasis on the stratotype locality at Frenchman Mountain.

METHODS

This paper is based primarily on traditional field measurements, using a Jacob staff calibrated in decimeters, and field descriptions of nine stratigraphic sections. The studied localities lie on an 85-km-long east-west transect that straddles the boundary between the Colorado Plateau and Basin and Range provinces. Sections extend from the Palisades of the Desert in eastern Grand Canyon to Frenchman Mountain adjacent to Las Vegas (Fig. 1). We also include stratigraphic data from the Nopah Range in California and from a tenth Tonto Group section, Blacktail Canyon in Arizona, which was measured and described by Rose (2003, 2006, 2011); the Blacktail Canyon locality is significant because it was proposed by Rose (2011) as the type section of the Tonto Group (as originally defined). Detailed locality data and detailed descriptions of measured sections in the western Grand Canyon and Lake Mead regions are available in Korolev (1997, his appendix A), with the exception of sections at Palisades of the Desert and Fern Glen Canyon. The Palisades of the Desert section was measured near the top of a talus cone on the east side of the Colorado River at 36.14226°N, 111.80489°W. Stratigraphic details of the Fern Glen Canyon section are in Rowland et al. (1995). Petrographic thin sections of representative facies were examined and described by Korolev (1997; see also Brathovde, 1986).

Hand samples for carbon isotope chemostratigraphy were collected every 1 m in the Lyndon Limestone Member of the Bright Angel Formation and every 1.5 m within the Muav Formation, FMD, and Nopah Formation. These samples were petrographically screened by comparing the least-altered phases in thin section to their counterpart billets so that we could microdrill the least-altered phases from the billets, avoiding late-stage spar, crusts, fossils, and allochems. In dolostones, including the FMD, dolomicrite (1–4 µm grain diameter), dolomicrospar (5–20 µm), and dolomitic oolite (0.5–2 mm) were drilled, yielding ~1 mg of powder. Stable isotope ratios ($\delta^{18}O$ and $\delta^{13}C$) were measured on ~300 µg of powder using two different systems at the University of Arizona Environmental Isotope Laboratory. Some samples were measured using an automated carbonate preparation device (Kiel III) coupled to a gas-ratio mass spectrometer (Finnigan MAT 252). In this system, powdered samples were reacted with dehydrated phosphoric acid under vacuum at 70 °C. Some samples were measured using a GasBench continuous flow headspace sampler connected to a Thermo-Finnigan Delta-Plus mass spectrometer. These samples were reacted overnight at room temperature with dehydrated phosphoric acid in He-filled vials, after which the evolved CO_2 was transferred to the mass spectrometer using a He-carrier gas. The isotope ratio measurement was calibrated based on repeated measurements of the NBS-19 and NBS-18 reference materials and of CAR2, an in-house carbonate standard. The following isotope ratios are assigned to these standards ($\delta^{18}O$ followed by $\delta^{13}C$): NBS-19, –2.20‰, +1.95‰; NBS-18, –23.20‰, –5.01‰; and CAR2, –1.41‰, +2.03‰. Analytical precision is ±0.10‰ for $\delta^{18}O$ and ±0.08‰ for $\delta^{13}C$ (1σ) for the Kiel III system; in the GasBench system, analytical precision is ±0.15‰ for $\delta^{18}O$ and ±0.10‰ for $\delta^{13}C$ (1σ). Replicate samples were analyzed, one in each system, to ensure similarity of results. The complete data set, including precision for each analytical run, is available as Table S1 in the Supplemental Material[1].

To evaluate the level of order present in the arrangement of FMD strata, and specifically the presence of cyclicity, we used the nonparametric statistical method of Burgess (2016). This method has two components. The first component—the Markov order metric—uses the observed facies succession pattern to evaluate the orderliness of the succession. The value of the metric m is between 0 (for perfectly disordered strata) and 1 (for perfectly ordered strata). The second component—the runs order metric—uses the pattern of increasing or decreasing thickness of the strata to evaluate their orderliness. The runs order metric r typically takes a value of $1 < r < 2$ (for perfectly disordered strata thicknesses) and $2 < r < 3$ (for perfectly ordered thicknesses). For each of these metrics, the corresponding P-value was obtained using a Monte Carlo approach based on 5000 random shuffles of the observed data. All of the analyses were run using the OrderID Matlab code available at https://csdms.colorado.edu/wiki/Model:OrderID. For the purposes of this analysis, the uppermost 52 m of the Frenchman Mountain section was not included. This interval consists of a single facies—glauconitic, bioclastic grainstone—which occurs only in this uppermost interval.

RESULTS AND INTERPRETATIONS

Stratigraphy

McKee (1945, p. 77–78) described three types of dolostone within his undifferentiated dolomites:

[1]Supplemental Material. Figure S1: Detailed stratigraphic column of stratotype. Figure S2: Carbon and oxygen isotope data plotted stratigraphically and also graphed against each other. Table S1: Table of carbon and oxygen isotope data. Please visit https://doi.org/10.1130/GEOS.S.21860211 to access the supplemental material, and contact editing@geosociety.org with any questions.

"(1) a white to buff, granular, hard, massive dolomite; (2) a white to yellow, aphanitic (porcelain-textured), thin-bedded dolomite showing fine, irregular laminae on weathered surfaces; and (3) steel-gray, fine-grained, thick-bedded dolomite which weathers with olive, silty surfaces and forms resistant cliffs." These lithologies are consistently distinct from the limestones and dolostones of the underlying Muav Formation, which is why McKee decided to exclude them from the Muav. The carbonates at the top of the Muav are typically darker and more resistant to erosion than those at the base of the FMD. However, the contact between the Muav and the FMD is not simply a contact between limestone and dolostone. The uppermost Muav is also dolostone in many Grand Canyon sections, and it is consistently dolostone in the western Grand Canyon and Lake Mead region (Korolev, 1997) (Fig. 1). In Marble Canyon, in a fault-controlled side canyon (informally named "50-Mile creek"), on the west side of the Colorado River, 49.7 river miles below Lee's Ferry, the carbonates of the Muav Formation transition into a siliciclastic facies below the dolostone of the FMD (Fig. 1). At some western localities, such as Diamond Bar Ranch, Arizona, the top of the Muav is characterized by karstic features: cracks with brecciated and terra rossa–like infill. This surface is capped by laminated to stromatolitic dolostones of the basal FMD. Together, these characteristics intimate the presence of a subaerial exposure surface and flooding event at the Muav-FMD contact.

In the Grand Canyon, the FMD forms westward-thickening vertical cliffs between the top of the Muav Formation and the base of the Devonian Temple Butte Formation (Fig. 3). In most sections examined in this study, the Havasu Member of the Muav, which directly underlies the FMD, is also dolomitized, but the boundary is usually unambiguous and sharp in the field. In western Grand Canyon and Lake Mead region sections, we identify the base of the FMD as an interval dominated by dololaminite, with or without stromatolites. This interval is lighter in color and less resistant to erosion than are the underlying beds of the Muav Formation. Also, in most western sections, beginning with those exposed in Quartermaster Canyon and the informally named "269-Mile canyon" (located on the north side of the Colorado River, 269.3 river miles downstream from Lee's Ferry), and continuing westward, chert nodules are conspicuously present within the basal few meters of the FMD (Figs. 1 and 4). In the eastern Grand Canyon, the presence of meter-scale stratigraphic couplets is a distinguishing feature of the FMD.

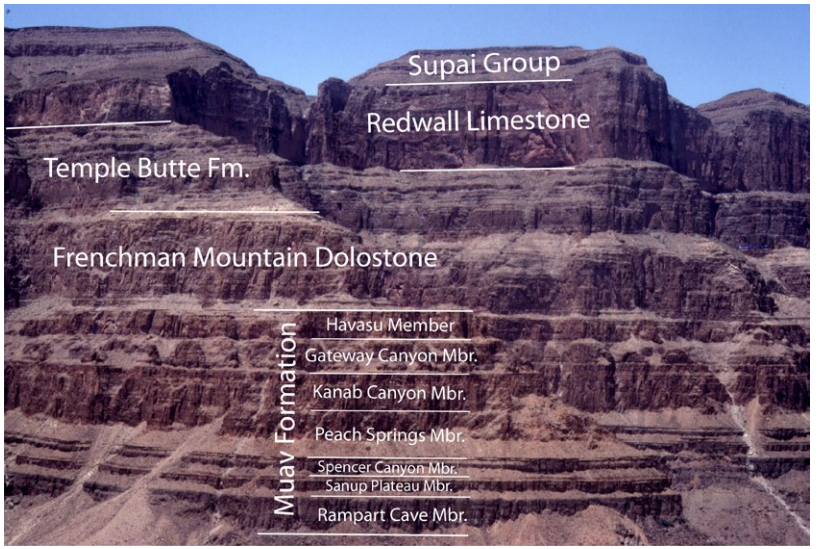

Figure 3. Quartermaster Canyon (Arizona) exposure, with stratigraphic units labeled. The Frenchman Mountain Dolostone here is 117 m thick. View is toward the west.

On the basis of lithostratigraphic characteristics, we can correlate the FMD 280 km westward from the eastern Grand Canyon to the edge of the Cambrian craton and an additional 100 km onto the shelf (Fig. 1). Southern Great Basin localities have had a complex structural history. Craton-margin sections experienced Neogene westward extension (Wernicke et al., 1988), and shelf sections experienced both eastward Cretaceous thrusting (Levy and Christie-Blick, 1989) and Neogene extension. Thus, the relative Cambrian positions of some of these sections are not precisely known. The pre-extension position of Frenchman Mountain, however, has been reconstructed with a high degree of confidence (Fryxell and Deubendorfer, 2005).

The base of the FMD correlates with a third-order sequence boundary recognized by Keller et al. (2012) ~130 m above the base of the Banded Mountain Member of the Bonanza King Formation in the Nopah Range (Fig. 1). Montañez and Osleger (1993) did not recognize discrete sequence boundary surfaces within the Bonanza King Formation. Rather, they identified "sequence boundary zones," which are intervals of thin, tidal flat–dominated parasequences that exhibit evidence of multiple episodes of exposure. In the Nopah Range, and also at Indian Ridge, Nevada, one of their sequence boundary zones occurs ~130 m above the base of the Banded Mountain Member. This interval is hypothesized to be correlative with the 130 m sequence boundary recognized by Keller et al. (2012).

A stratigraphic interval that has proven to be helpful in constraining the portion of the Bonanza King Formation that correlates with the FMD is a distinctive, reddish, silty interval at the base of the Banded Mountain Member. This reddish silty interval was recognized by Hazzard and Mason (1936), who informally named it "Member 2" in

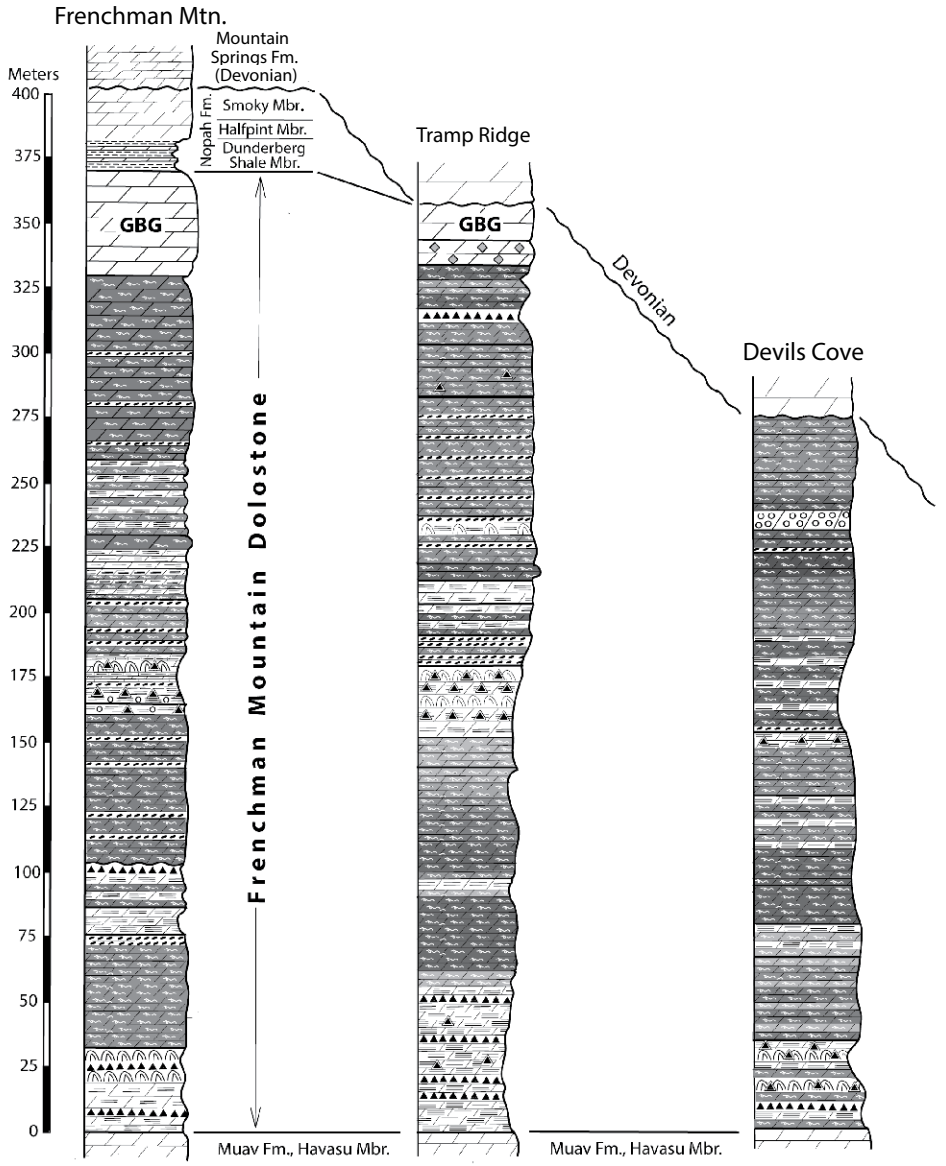

Figure 4. Stratigraphic columns and weathering profiles of Frenchman Mountain Dolostone exposures in the Lake Mead region and western Grand Canyon. GBG—glauconitic bioclastic grainstone; FM—Frenchman Mountain, Nevada; TR—Tramp Ridge, Nevada; DC—Devils Cove, Nevada; DBR—Diamond Bar Ranch, Arizona; 269—269-Mile canyon, Arizona; QM—Quartermaster Canyon, Arizona; FG—Fern Glen Canyon, Arizona; BT—Blacktail Canyon, Arizona; PAL—Palisades of the Desert, Arizona; 50—50-Mile creek Canyon, Arizona. Varying shades of gray displayed in the burrow-mottled dolostone lithology symbolize variation in the darkness of this facies. (*Continued on following page.*)

their original description of the Bonanza King Formation in the Providence and Marble Mountains of California. Barnes and Palmer (1961), working at the Nevada Test Site, later used this same interval to formally subdivide the Bonanza King Formation into two members: the Papoose Lake Member below and the Banded Mountain Member above. The silty carbonate interval defines the basal portion of the Banded Mountain Member. Osleger and Montañez (1996) referred to this interval as their "mixed unit," interpreting the abundant quartz silt to represent eolian dust that was blown onto carbonate tidal flats from the non-vegetated Laurentian craton. Keller et al. (2012) referred to this interval as the "silty interval," a term we use as well (Fig. 1). We interpret this silty interval to represent a lowstand systems tract that overlies the sequence boundary identified by Keller et al. (2012) in the Nopah Range (Fig. 1). We follow Osleger and Montañez (1996) and Keller et al. (2012) in employing this reddish siltstone as a geologically isochronous interval.

At Frenchman Mountain and Diamond Bar Ranch, a prominent reddish, silty interval occurs within the upper portion of the Kanab Canyon Member of the Muav Formation and also in the overlying Gateway Canyon Member (Figs. 1 and 3). The red color continues less prominently into exposures of the overlying Havasu Member. These lowstand-systems-tract red silts were presumably removed by erosion in more cratonward sections. We correlate this interval with the silty interval at the base of the Banded Mountain Member of the Bonanza King Formation, permitting a robust correlation between the shelf and the sparsely fossiliferous and unfossiliferous strata on the craton at this stratigraphic position. Its position is also bracketed by distinctive chemostratigraphic trends in these successions, observed by Montañez et al. (2000), Lin et al. (2019), and this study (see below). Together, such evidence supports correlation of the boundary between the Muav Formation and the Frenchman Mountain Dolostone with the third-order sequence boundary located a few tens of meters above the top of the reddish silty interval of the Banded Mountain Member, as identified by Osleger and Montañez (1996) and Keller et al. (2012).

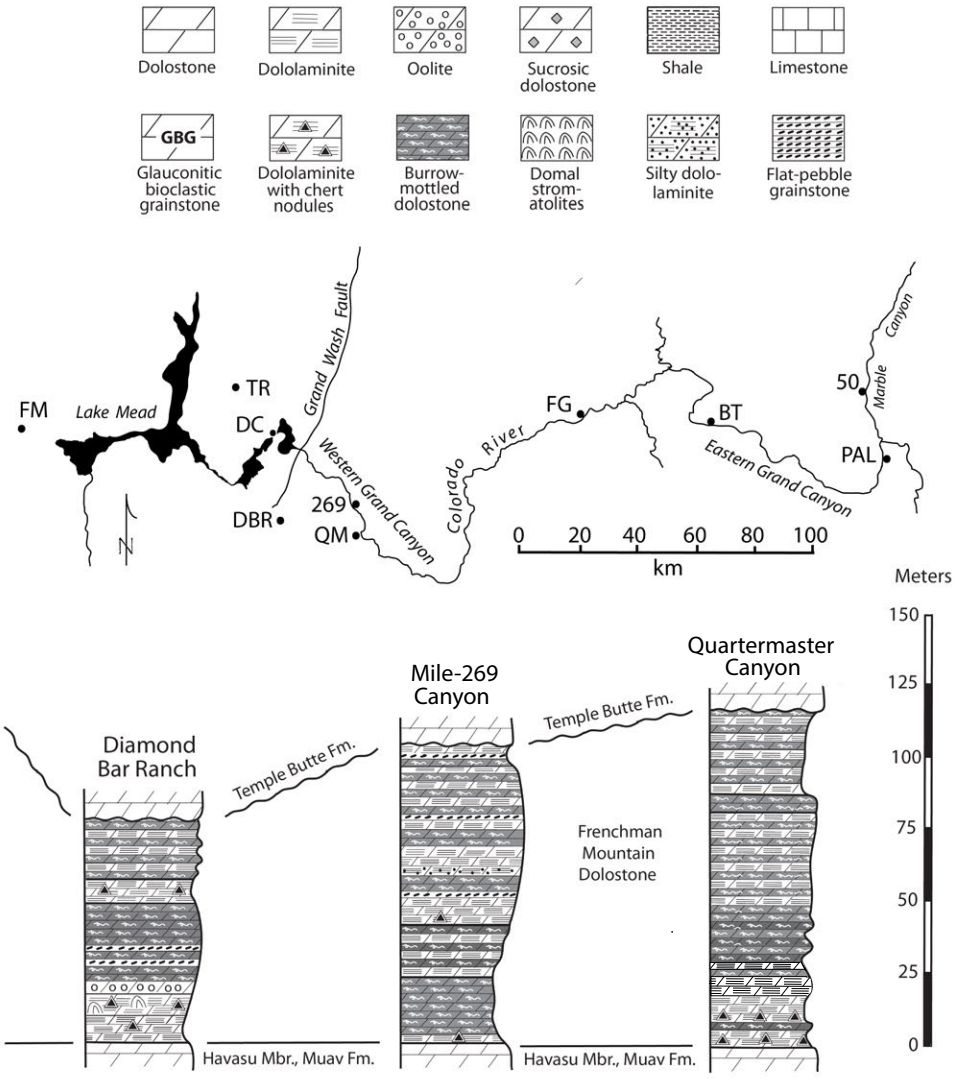

Figure 4 (*continued*).

From a thickness of 371 m at the stratotype section at Frenchman Mountain, the FMD thins eastward to 362 m at Tramp Ridge and 274 m at Devils Cove (Fig. 1). East of the Grand Wash fault, thicknesses decrease sharply (Fig. 1) to 117 m at Quartermaster Canyon, 106 m at 269-Mile canyon, and 77 m near Diamond Bar Ranch. Eastward into the Grand Canyon, the thickness gradually decreases to 52 m in Fern Glen Canyon (Rowland et al., 1995) and 20 m at Blacktail Canyon (Rose, 2003, 2011). The abrupt change in thickness across the Grand Wash fault suggests that this fault was active during the Cambrian Period.

In its easternmost exposures, in Marble Canyon, the FMD varies from 30 m in thickness at 50-Mile creek to just 8 m at Palisades of the Desert (Fig. 5). The thinness of the FMD in the Palisades of the Desert section is due to the presence of an incised valley filled with the Devonian Temple Butte Formation. Pre–Temple Butte incision of this valley removed at least 12 m of the FMD (Fig. 5).

Facies and Depositional Environment Interpretations

Brathovde (1986) found the FMD in Grand Canyon exposures to be pervasively dolomitized—predominantly composed of dolomicrite—with the original textures obliterated beyond recognition. However, in exposures in the Lake Mead region, including the Frenchman Mountain stratotype section, the original sedimentary textures are mostly preserved, despite dolomitization.

We recognize the following eight lithofacies in the FMD, representing peritidal and shallow subtidal depositional environments: (1) cryptomicrobial dololaminite (with or without associated chert nodules and with or without mudcracks and/or tepee structures), (2) silty dololaminite, (3) flat-pebble conglomerate, (4) rippled dolostone, (5) burrow-mottled mudstone and wackestone, (6) stromatolitic boundstone, (7) oolitic grainstone, and (8) glauconitic bioclastic grainstone (Fig. 6). Carbonate lithologic terminology follows Dunham (1962). Each of these lithofacies is briefly described and interpreted in the following sections.

(1) Cryptomicrobial Dololaminite (Figs. 6A and 6B)

This facies consists of planar-parallel and wavy-parallel, light gray, finely laminated (0.5–2.0 mm) dolomitic mudstone-wackestone and interbedded flat-pebble conglomerate. It occurs in all sections, most commonly in the lower portion of the FMD as lithologically distinct, recessive intervals, ranging from 5 to 20 m in thickness. Buff to yellowish brown chert lenses are common, typically with laminae preserved within the chert (Fig. 6A).

In some cases, the laminae display occasional disruptions, desiccation features, and evidence of traction deposition, such as low-angle truncations. Thin, 2- to 8-cm, intraclastic beds are common. Desiccation features, such as mudcracks, micro-erosion surfaces, and tepee structures, are commonly present (Fig. 6B). This facies is typically closely associated with low-profile, laterally linked stromatolites (Fig. 6C). This facies is a ubiquitous component of carbonate platform deposits (e.g., Barnaby and Read, 1990; Zhang et al., 2015; Guo et al., 2018a; Pratt and Rule, 2021).

We interpret this facies to be the product of sediment trapping and binding by microorganisms and/or biologically induced direct precipitation of calcium carbonate from the water column on periodically exposed tidal flats (Assereto and Kendall, 1977; Shinn, 1983; Burne and Moore, 1987; Noffke and Awramik, 2013).

(2) Silty Dololaminite (Fig. 6D)

This is a mixed facies of interlaminated quartz silt and dolomicrite occurring in centimeter- and millimeter-scale couplets, displaying wavy-parallel and planar-parallel laminations. Asymmetric, climbing ripples are common, with centimeter-scale amplitudes and wavelengths in the range of 5–8 cm (Fig. 6D). This facies forms a significant

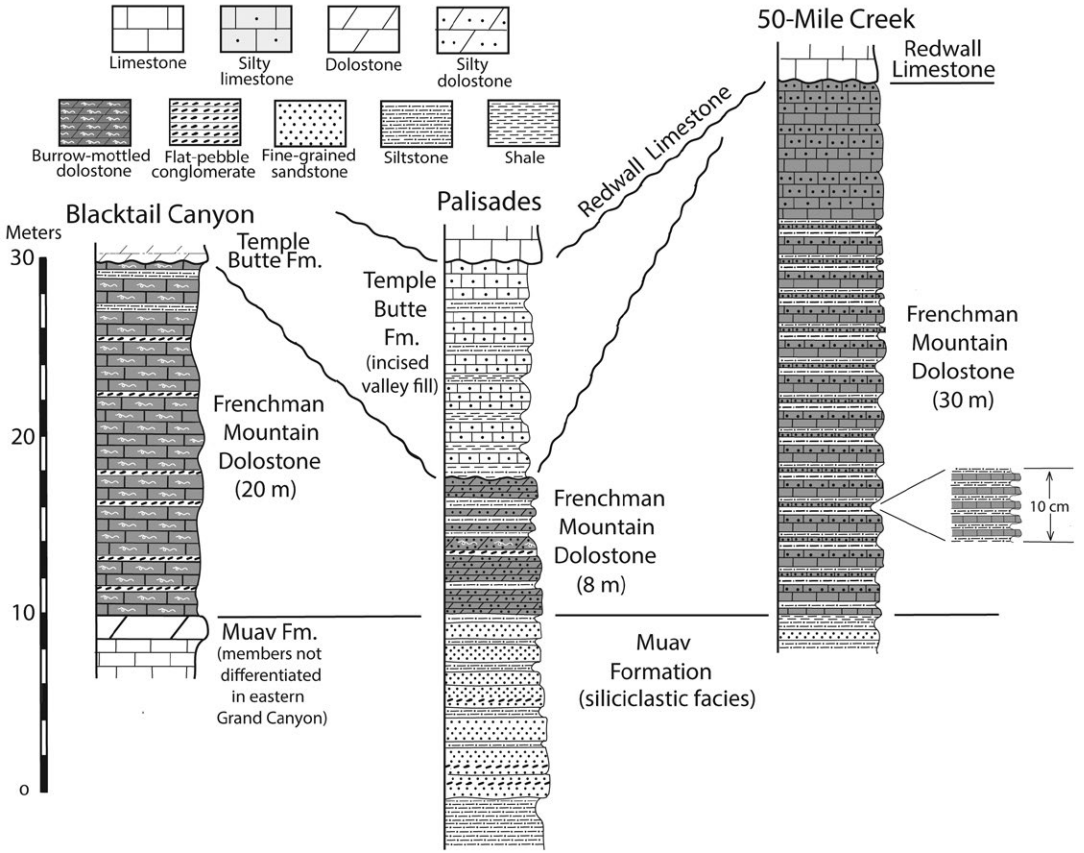

Figure 5. Stratigraphic columns and weathering profiles of Frenchman Mountain Dolostone exposures in eastern Grand Canyon. See Figure 4 for column locations.

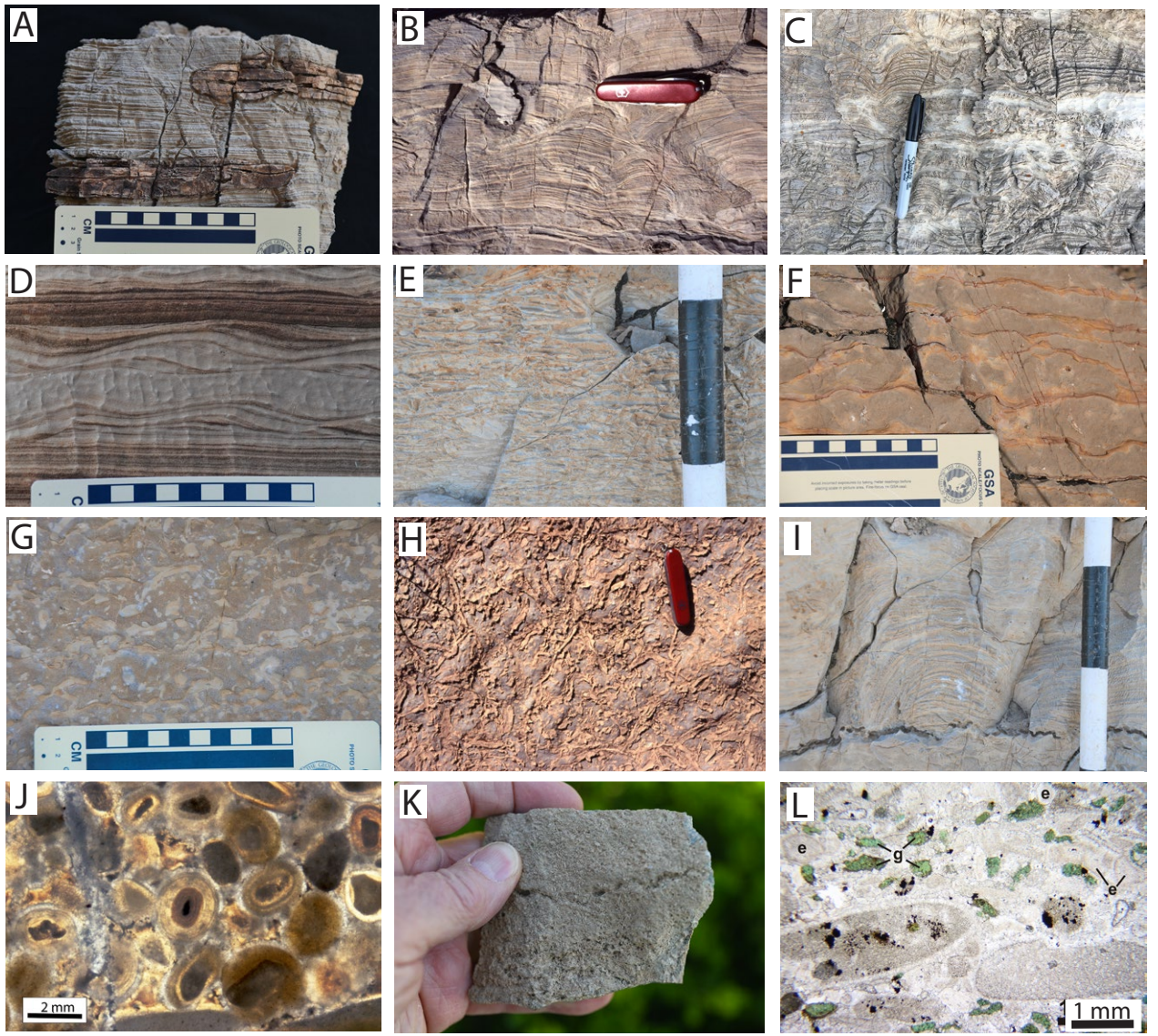

Figure 6. Images of lithofacies in the Frenchman Mountain Dolostone. (A) Cryptomicrobial dololaminite with chert nodules; Frenchman Mountain, Nevada. (B) Dololaminite with tepee structures; 269-Mile canyon, Arizona. Knife is 9 cm long. (C) Laterally linked stromatolites; Frenchman Mountain. Marker is 13.5 cm long. (D) Silty dololaminite; Frenchman Mountain. Scale in centimeters. (E) Flat-pebble conglomerate; Frenchman Mountain. Black interval on staff is 10 cm. (F) Rippled dolostone; Frenchman Mountain. Scale in centimeters. (G) Burrow-mottled mudstone; Frenchman Mountain. (H) Burrow-mottled mudstone, bedding-plane view; Diamond Bar Ranch, Arizona. Knife is 9 cm long. (I) Stromatolitic boundstone; Frenchman Mountain. Black interval on staff is 10 cm. (J) Oolitic grainstone (thin section); Frenchman Mountain. (K) Glauconitic bioclastic grainstone; Frenchman Mountain. (L) Glauconitic bioclastic grainstone (thin section); Frenchman Mountain. g—glauconite; e—echinoderm plate; large oval structures are intraclasts.

component of the "silty interval" at the base of the Banded Mountain Member of the Bonanza King Formation (Fig. 1) (Osleger and Montañez, 1996). In the FMD, it is present only sporadically, and is rarely thicker than a few decimeters.

The quartz silt in this facies probably arrived in the carbonate peritidal environment as eolian dust from the craton, as suggested by Osleger and Montañez (1996). The silt was then intermingled with lime mud and reworked by tidal currents. It was ultimately deposited on tidal flats as laminated and rippled laminae.

(3) Flat-Pebble Conglomerate (Fig. 6E)

The flat-pebble conglomerate facies typically occurs as relatively thin (5–30 cm) beds of poorly sorted, partially imbricated, flat pebbles of chert and dolomicrite. Beds as much as 1 m thick in some cases occur. Pebbles are typically 2–5 cm long and <0.5 cm thick with rounded margins.

Flat-pebble conglomerates are common in Proterozoic and lower Paleozoic shallow-water carbonate deposits resulting from multiple processes (Lee and Kim, 1992; Myrow et al., 2004). In the case of the FMD, we interpret this facies to record the episodic occurrence of high-energy storm waves that ripped up and displaced portions of the intertidal and shallow-subtidal seafloor.

(4) Rippled Dolostone (Fig. 6F)

This facies consists of thin (1–8 cm), rippled, graded dolostone beds. The bases of the beds are coarse grained, and the rippled tops are composed of silty carbonate. These even, wavy-parallel beds are separated by very thin laminae (<2 mm) of nonresistant silty carbonate. The bottom of each bed reflects the morphology of the underlying rippled surface. Ripples with symmetrical crests are common, and ripple heights are 1–2 cm with an average wavelength of 6–7 cm. In some instances, a secondary crest, nearly perpendicular to the primary trend, is superimposed on the primary ripple crests, producing ladderback ripples on the bedding surface. Some ripples exhibit desiccation cracks on their crests. Some beds in this facies are moderately burrow mottled. This facies is commonly closely associated with the silty dololaminite facies. A similar facies has been described in other carbonate platform deposits (e.g., Chaudhuri, 2005).

We interpret this facies to record deposition in a peritidal setting, as indicated by the abundance of desiccation features, ladderback ripples, and a close association with the silty dololaminite facies. The conspicuous symmetrical ripples may record the influence of storm waves or possibly waves generated under slack-water conditions at high tide.

(5) Burrow-Mottled Mudstone and Wackestone (Figs. 6G and 6H)

The burrow-mottled facies, consisting of medium to dark gray, thick-bedded, burrow-mottled dolomitic mudstone and wackestone, is the volumetrically dominant facies within the FMD. It is common in Grand Canyon sections as well as those in the Lake Mead area. In Lake Mead region sections, this facies typically composes ~50% of the entire thickness of the formation. It is commonly intercalated with other facies; however, in Lake Mead region exposures, it commonly occurs in continuous intervals as much as 30 m in thickness. For the Muav Formation, McKee (1945) used the terms "marbled" and "mottled" to describe this facies.

In moderately burrowed examples of this facies, individual burrows are typically 1.5–2 cm in diameter and 7–10 cm long. They are commonly oriented vertically to subvertically. However, in more intensively burrowed examples, horizontal burrows are common (Fig. 6H). In addition to these large burrows, narrower burrows, 2–3 mm in diameter and 3–5 cm long, also occur.

The burrows, which were originally filled with lime mud, are now composed of coarse calcite mosaic, which makes them distinctly lighter in color than the surrounding matrix. As described by Brathovde (1986), the burrow-mottled facies most commonly has a crystalline mosaic texture represented by xenotopic dolomite and calcite crystals with irregular and curved intercrystalline boundaries and undulatory extinction. In most exposures, this facies is fairly homogeneous and exhibits no primary structures other than the burrows. The burrowing organisms presumably destroyed preexisting sedimentary structures.

The predominance of lime mud and burrow mottling, the rarity of cross-stratification, and the absence of exposure features all indicate deposition of this facies in a quiet, subtidal setting that was occasionally interrupted by storm events that produced interbedded flat-pebble conglomerates.

(6) Stromatolitic Boundstone (Fig. 6I)

This facies includes relatively large, domal stromatolites (Fig. 6I) as well as lower-profile forms. In Grand Canyon sections, the laminae rarely form domes. In more distal craton-margin sections, such as at Frenchman Mountain and Tramp Ridge, the stromatolites more commonly take the form of 5-cm- to 2-m-tall domes or slightly branching columns. Within this facies, orange to dark brown silicification is common, resulting in abundant chert nodules and lenses and silicified portions of stromatolites.

We distinguish two subfacies of this facies: one with high-profile domal forms and the other with low-profile, laterally linked forms that grade into parallel laminae. The former is most commonly associated with the burrow-mottled and oolitic grainstone facies.

We interpret the domal stromatolites to have formed in a quiet, subtidal setting where microorganisms baffled the water current and trapped sedimentary particles in a tangle of filaments (Noffke and Awramik, 2013). The lower-profile subfacies, in contrast, is more commonly associated with flat-pebble conglomerate; we interpret these low-profile stromatolites to have developed in a shallower, more energetic, peritidal environment. In such settings, in Cambrian platform deposits, stromatolites are very common (e.g., Zhang et al., 2015).

(7) Oolitic Grainstone (Fig. 6J)

Oolitic grainstones are not abundant in the FMD, although they become a dominant facies in

the uppermost hundred meters of the correlative Bonanza King Formation in southern Great Basin sections (Montañez and Osleger, 1993). Montañez and Osleger (1993, their figure 12) reported an interval ~40 m thick of their oolitic-skeletal shoal facies at Frenchman Mountain. Our Frenchman Mountain measured section, which we presume to be a different section than the one measured by Montañez and Osleger (1993), contains several meter-scale intervals of oolite but no interval that is tens of meters in thickness (Fig. 7). The thickest occurrence we encountered in this study is an 8-m-thick, laterally continuous interval in our Devils Cove section. More commonly, ooid-rich intervals occur within individual stromatolite beds and in burrow-mottled intervals.

Oolitic beds are composed of oolitic-intraclastic grainstone and packstone. The grains are poorly sorted, with ooids ranging from 0.5 to 2.0 mm in diameter and intraclasts ranging from subrounded 2 mm grains to elongate clasts as much as 1 cm in length (Fig. 6J). All ooids display concentric laminae, and most have micritic envelopes. Paleocurrent data from this facies, based on measurements of cross-stratified beds at Quartermaster Canyon and at Whitney Ridge, Nevada, indicate bimodal paleoflow with preferential NE-SW orientation (Korolev, 1997).

We interpret the depositional environment that produced this facies to have been subtidal, oolitic shoals that were open to the sea. Open-marine conditions favor the growth of tangentially oriented calcite crystals (Heller et al., 1980), such as those present in the FMD. The NE-SW bimodal orientation of paleocurrents is at a high angle to the Miaolingian shoreline of the Colorado Plateau region. Thus, we infer that the paleocurrents that are preserved as cross-bedding in the oolite grainstone record the action of tidal currents reworking ooid-shoal grains.

(8) Glauconitic Bioclastic Grainstone (Figs. 6K and 6L)

The glauconitic bioclastic grainstone facies is restricted to distal craton-margin sections where it forms very distinct, weakly stratified, reddish orange– to buff-weathering cliffs at the very top of the FMD. At Frenchman Mountain, this interval is 52 m thick. Its easternmost occurrence is at Tramp Ridge (Fig. 4), although it may have been present at more cratonward locations as well prior to the truncation of those sections by pre-Devonian erosion. But this facies is much less prominent, or completely absent, in shelf sections to the west. Gans (1974) reported no such facies in his stratigraphic study of Bonanza King Formation exposures in the upper plate of the Keystone thrust in southern Nevada, nor did Fenton (1980) report this facies in the Bonanza King Formation in the Desert Range, Nevada. Montañez and Osleger (1993) reported an ooid-skeletal-shoal facies at the correlative position at the top of the Bonanza King in sections to the west but not in thicknesses comparable to those at Frenchman Mountain.

Bioclasts in this facies are predominantly flat, millimeter-scale plates (Fig. 6L). In thin section, in polarized light, the plates exhibit uniform extinction and a perforate fabric typical of stereom. These characteristics unequivocally identify the bioclasts as echinoderm ossicles (Bathurst, 1972). Although we cannot rule out the possibility that these ossicles represent stylophorans, they probably represent eocrinoids, a group of mostly stalked, high-level suspension feeders that were abundant in the Miaolingian and Furongian of western North America (Robison, 1965; Sprinkle and Kier, 1987). Eocrinoids commonly occurred in gregarious associations (Sprinkle and Kier, 1987) and could produce encrinite-like facies such as this one. Extant echinoderm taxa have a low tolerance for salinity variations (Sprinkle and Kier, 1987), and it is commonly inferred that this limitation applies to the phylum as a whole. Thus, the abundance of echinoderm skeletal grains in this facies implies normal marine salinity. Rare elongate trilobite fragments are present in thin sections. Bioclastic grainstone is the dominant lithology in this facies, but wackestone and packstone also occur. Pore space is occluded with a fine, microspar mosaic.

Deep green, rounded, millimeter-scale peloids of the micaceous mineral glauconite are abundant at the base of the thick interval composed of this facies and are uniformly dispersed among the hypothesized eocrinoid plates (Fig. 6L). The glauconite grains become progressively less abundant upsection within the 52 m interval, and they are rare to absent at the top. In modern seas, glauconite forms in relatively deep water (Cloud, 1955). However, it is conspicuously abundant in Cambrian shallow-water sediments. Peters and Gaines (2012) attributed this anomaly to enhanced chemical weathering of continental crust globally, associated with the development of the Great Unconformity (see also Rowland, 2022).

Glauconite peloids, such as those in this facies, are commonly interpreted to be altered fecal pellets. Filter-feeding organisms, such as eocrinoids, remove clay and silt-size particles from the water column, producing fecal pellets of clay aggregates that are diagenetically altered to glauconite (Chafetz and Reid, 2000; see also El Albani et al., 2005). We suggest that the glauconite peloids in this facies probably resulted from that process. The low faunal diversity suggests a restricted environment, however the abundance of echinoderms implies normal marine salinity such as might occur in a coastal embayment.

The lack of desiccation features and absence of distinct bedding suggest a subtidal environment, while the fragmented bioclastic grains suggest the occasional presence of moderate- to high-energy storm waves. We suggest that this facies records the presence of an extensive, long-lived, subtidal, eocrinoid-rich embayment.

Sequence Stratigraphy, Stacking Patterns, and Facies Couplets

We recognize six depositional sequences within the FMD at Frenchman Mountain (Fig. S1). As is typical of shallow carbonate platforms, however, each sequence is not bounded by a single, unambiguous erosion surface (Strasser, 2015). Rather, there are sequence boundary "zones," each consisting of stacked amalgamations of minor erosion surfaces, dololaminites, and stromatolitic facies (Fig. 7; Fig. S1). Sufficient ambiguity exists regarding where to define a sequence boundary in such situations that different researchers may identify

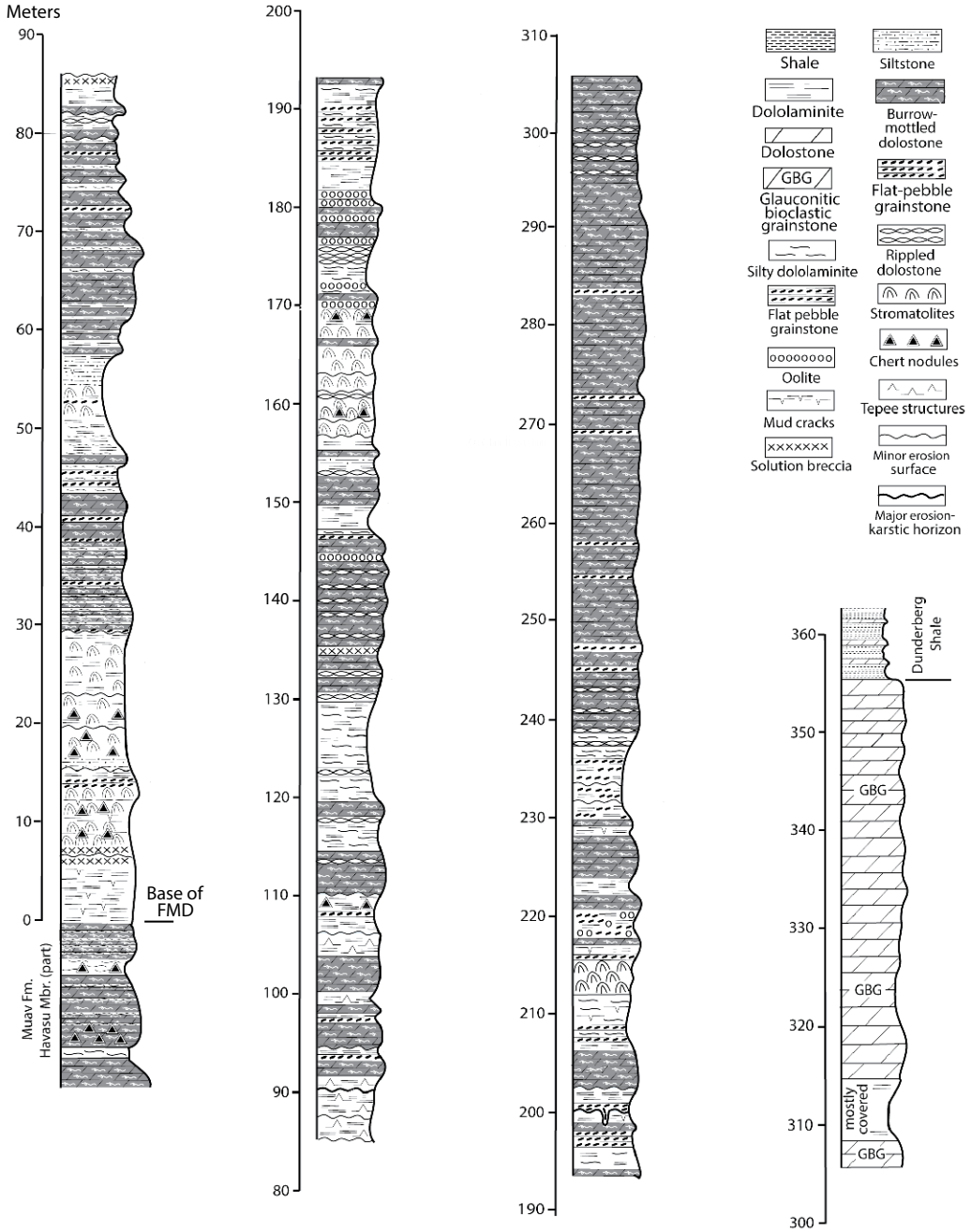

Figure 7. Stratigraphic column and weathering profile of the Frenchman Mountain Dolostone (FMD) stratotype at Frenchman Mountain, Nevada. GBG—glauconitic bioclastic grainstone.

sequences differently. Montañez and Osleger (1993), for example, recognized just three sequences within the FMD at Frenchman Mountain (their Banded Mountain Member of Bonanza King Formation), in contrast to our six.

Figures 4 and 5 show supra-meter-scale occurrences of facies within the FMD at different localities. In contrast, a higher-resolution, meter-scale representation of facies within the Frenchman Mountain stratotype section is presented in Figure 7. At the supra-meter scale, intervals dominated by intertidal facies and those dominated by shallow-subtidal facies roughly correlate from one section to the next (Figs. 4 and 5). There is a no conspicuous pattern of lithologic cyclicity at this scale.

Supra-Meter-Scale Alternation of Subtidal Facies

Intervals of alternating subtidal facies are common in the FMD (Fig. 7). Each alternating couplet is typically several meters thick, composed of dark to medium gray, highly bioturbated, thick-bedded, dolomitic mudstone, gradationally overlain by one or another of three facies: (1) less-bioturbated, thinner-bedded, medium gray dolomitic mudstone, (2) a layer of laterally linked stromatolites, or (3) silty dololaminite (Fig. 7). The upper facies is then overlain by intensively burrow-mottled mudstone, which begins the next couplet. Evidence of erosion or subaerial exposure is lacking in these intervals.

Meter-Scale Peritidal Facies Couplets

Meter-scale couplets of alternating peritidal facies are ubiquitous components of carbonate platforms (e.g., Osleger and Read, 1991; Montañez and Osleger, 1993; Meng et al., 1997; Wilkinson et al., 1998; Lehrmann and Goldhammer, 1999; Burgess, 2006; Zhang et al., 2015; Guo et al., 2018a, 2018b), They conspicuously occur within the FMD (Figs. 7 and 8A–8F) as well as within correlative portions of the Bonanza King Formation. Distinctive dark-and-light bands exposed on Banded Mountain in Nye County, Nevada, provided the name of the Banded Mountain Member of the Bonanza King Formation, the unit that is partially correlative with the FMD (Fig. 1).

In the FMD, each dark-and-light couplet is typically one to two meters thick (Figs. 8A–8F). The dark interval is medium to dark gray, intensively burrowed mudstone (burrow-mottled facies), in some cases interbedded with silty dololaminite (Fig. 8E). High-relief, laterally linked stromatolites as well as rippled dolostone rarely occur in the basal portion

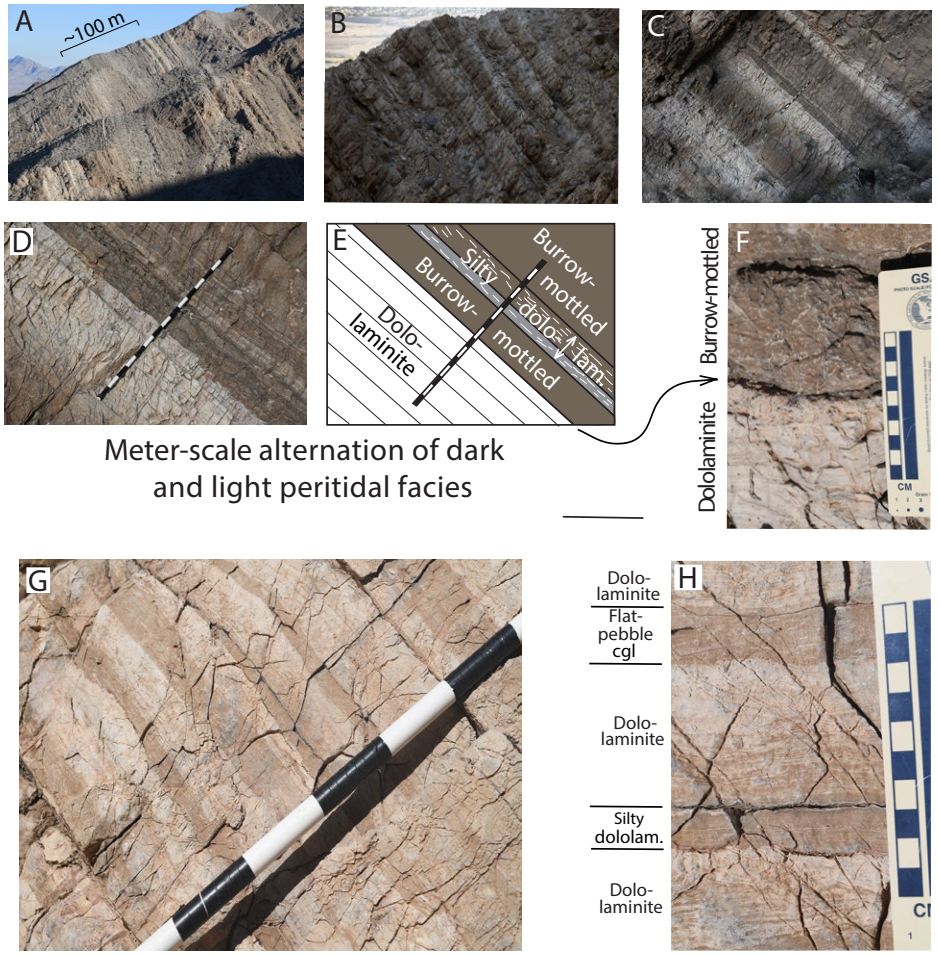

Figure 8. Meter-scale and decimeter-scale facies couplets in the Frenchman Mountain Dolostone at Frenchman Mountain. (A) General view toward the north from the central part of the mountain, east of East Bonanza Road. (B) Meter-scale peritidal couplets. (C–E) Meter-scale peritidal couplets. Staff is 1.5 m. (F) Detail of boundary between stacked, peritidal facies, with 10 cm scale. (G) Stacked decimeter-scale peritidal facies. Black and white intervals are each 10 cm. (H) Detail of decimeter-scale couplets, with 10 cm scale. cgl—conglomerate; dololam.—dolo-laminite.

of this dark band. Flat-pebble conglomerate commonly dominates the upper portion of this band.

Over a transition zone of one to two decimeters, the dark band typically grades into a light-colored band (Figs. 8B and 8C). The light-colored band is typically thinner than the dark band. It consists of silty dololaminite and/or dololaminite with mud cracks. Micro-erosional surfaces, karst features, and low-relief stromatolites are common in the lighter interval. In Grand Canyon exposures, where the bedding is horizontal, the meter-scale couplets typically form prominent cliff-and-slope topographic cycles. The burrow-mottled, darker portion of each couplet is less resistant to erosion than is the lighter portion, so the darker portion typically erodes more readily, forming a recess beneath the more resistant lighter interval.

There is a long history of discussion and debate concerning the origin of meter-scale variation in peritidal facies on carbonate platforms, with glacio-eustatic sea-level change commonly being the preferred mechanism (e.g., Osleger and Read, 1991; Montañez and Osleger, 1993; Meng et al., 1997; Strasser, 2015; Zhang et al., 2015; Guo et al., 2018a, 2018b). Inferred processes generating meter-scale cycles range from nearly random to deterministic in their temporal frequency (Lehrmann and Goldhammer, 1999), and some of the proposed processes may not be sensitive to water depth (Rankey, 2004) or wave height (Purkis et al., 2015). It has proven to be very challenging, therefore, to discern between the influence of externally driven, allocyclic forcing and that of inherent, autocyclic processes in the creation of alternating meter-scale couplets of peritidal carbonate facies preserved in the rock record (Wright and Burchette, 1996; Hill et al., 2009, 2012).

Peritidal couplets, such as those in the FMD, may not record actual changes in water depth; they may be a function of autocyclic processes that are unrelated to episodes of sea-level change. Such meter-scale couplets can be a product of random or nearly random patterns of lateral sediment transport as tidal flat islands accrete vertically and migrate laterally during relatively steady, passive-margin subsidence (Pratt and James, 1986; Wilkinson et al., 1998; Dyer and Maloof, 2015).

Decimeter-Scale Facies Couplets

Decimeter-scale couplets, 0.1 to 0.5 m thick, also occur in the FMD (Figs. 8G and 8H). They occur in light-colored, dololaminite-dominated intervals, but the suite of facies from which these cycles are constructed is variable. At Frenchman Mountain, the decimeter-thick couplets typically consist of silty dololaminite or flat-pebble conglomerate at the base, capped by cryptomicrobial laminite (Fig. 8H). At 269-Mile canyon and Quartermaster Canyon, the decimeter-scale couplets more commonly begin with a thin interval of burrow-mottled or nodular facies, capped by a thicker, cryptomicrobial interval with mud cracks. Low-relief stromatolites may occur at the bases of these couplets.

In our 50-Mile creek section, there is a striking example of centimeter- and decimeter-scale couplets nested within meter-scale alternations of facies. That section of the FMD consists of meter-scale couplets of siltstone and silty limestone with a very regular alternation of lithologies with respect to the abundance of silt (Fig. 5). Within the meter-scale fluctuations in silt abundance are centimeter-scale alternations; centimeter-scale limestone beds are interbedded with centimeter-scale siltstone intervals.

Statistical Analysis of Facies Succession Patterns and Thicknesses

The logged strata within the Frenchman Mountain stratotype section consist of 222 intervals of seven of the eight lithofacies described above (excluding the glauconitic bioclastic grainstone facies, which occurs in one continuous interval at the top of the Frenchman Mountain section) (Fig. S1, see footnote 1). The average stratum thickness is 1.36 m.

The null hypothesis is that there is no order in the sequence and thicknesses of these strata. Following Burgess (2016), we derived the Markov metric m from an analysis of the vertical succession of FMD facies, and the runs metric r from an analysis of the thicknesses of the units. This analysis involved a comparison of the values derived from the documented occurrences and thicknesses of strata in the measured stratotype section at Frenchman Mountain with 5000 randomly shuffled versions of the same set of strata. This provided a way to generate a suite of similar but disordered strata for comparison with the measured section.

The results are displayed in Figure 9. Figure 9A shows the vertical succession of facies. Figure 9B is a transition probability matrix of the facies, used to calculate the Markov metric. For example, there is a 38% probability of transitioning from facies 7 to facies 1. Figure 9C shows the frequency of the facies, irrespective of thickness. Figure 9D is a graph of the Markov order metric, with the red line indicating the observed value $m = 0.081$ (P-value 0.8274); the blue area shows the probability distribution of the metric based on 5000 random shuffles of the observed data. Figure 9E is a graph of the runs order metric r, with the red line indicating the observed value $r = 1.283$ (P-value 0.5324); the blue area shows the probability distribution of the metric based on 5000 random shuffles of the observed data.

P-values of 0.05 or less are generally considered to be statistically significant, which would providing support for the alternative hypothesis that there is order in the sequence and/or thickness of the succession of strata. The very high P-values obtained here do not permit the rejection of the null hypothesis of no order. We conclude, therefore, that there is no evidence for order, including cyclicity, in the stratigraphy of the FMD at Frenchman Mountain based on the applied metrics. This conclusion is visually reinforced by the graphs in Figures 9D and 9E, which show that the calculated Markov metric and runs metric values lie close to the center of the respective distributions generated from 5000 random shuffles of the observed data.

A study that is peripherally relevant to our study was conducted by Burgess (2008), in which he used data from Montañez and Osleger (1993) to analyze carbonate thickness distributions at Frenchman Mountain, among many other localities, in the Muav Formation and FMD (considered by Montañez and Osleger to be the Bonanza King Formation). Facies succession patterns, such as cyclicity, were not addressed in the Burgess (2008) study, only the distribution of bedding thickness.

Carbonate platforms commonly exhibit an exponential distribution of lithofacies thicknesses, with a high number of thin units and exponentially fewer intermediate and thick beds. However, Burgess found that the distribution of stratigraphic thicknesses in the Frenchman Mountain section, among other sites, did not conform to the predicted exponential distribution; there were too few thin units and too many intermediate and thick beds. A possible explanation suggested by Burgess (2008) is a measuring bias on the part of the stratigrapher; thin beds, especially of the same lithofacies, tend to be grouped together in the stratigraphic column. In our study of the FMD, such groupings of thin lithofacies units doubtless occurred. We measured our sections with a 1.5 m Jacob staff, and it was not practical, within a reasonable amount of time, to record decimeter-scale facies changes within a section that is hundreds of meters thick.

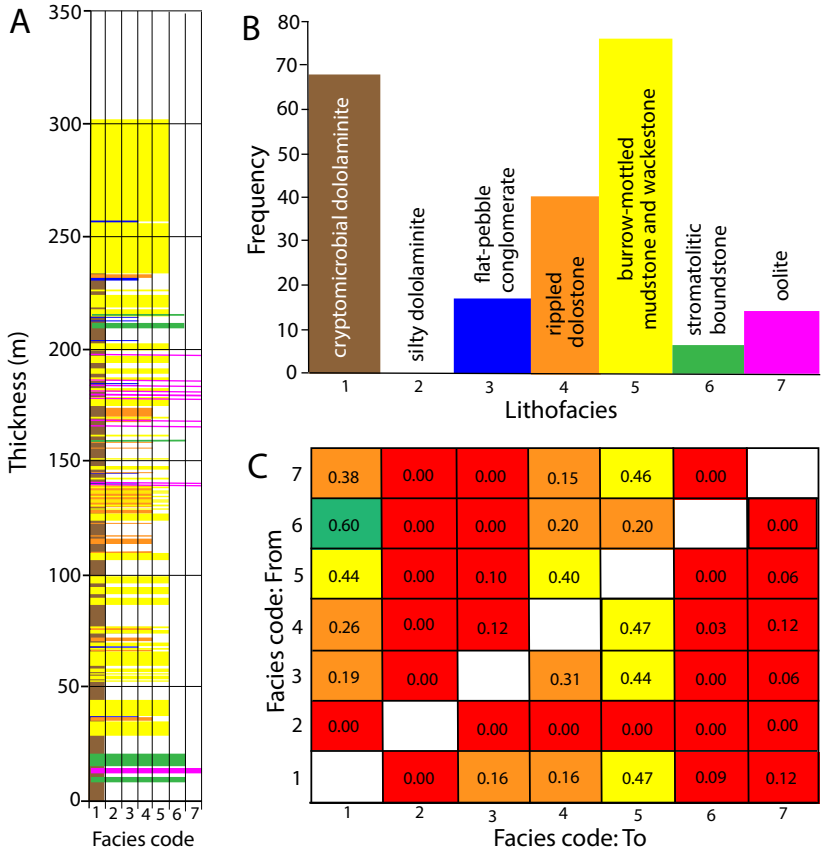

Figure 9. Graphical results of statistical analysis of orderliness and thickness patterns within seven facies of the Frenchman Mountain Dolostone in the Frenchman Mountain stratotype section. (A) Facies thickness pattern. Facies codes correspond with those shown in B. Facies 2 (silty dololaminite) is an uncommon facies and it rarely occurs in beds more than a few decimeters in thickness; at the scale represented in this column it does not appear, although it occurs in the data used to construct the transition probability matrix. (B) Histogram showing the frequency at which each facies occurs in the section, irrespective of its thickness. (C) Transition probability matrix of the seven facies used to calculate the Markov metric. For example, there is a 38% probability of a transition from facies 7 to facies 1. Colors identify levels of probability: green, 60%; yellow, 40–47%; orange, 15–38%; red, 0–6%. (*Continued on following page.*)

Autocyclic versus Allocyclic Processes in the Deposition of the FMD

There is general agreement that there was an absence of polar ice caps, sea ice, and continental ice in the Cambrian Period (Hearing et al., 2018; Wotte et al., 2019; but see Runkal et al., 2010, and response by Landing, 2011). Coupled with extremely high (~4500 ppm) atmospheric CO_2 (Berner and Kothavala, 2001), this indicates that the Cambrian Period, and the Miaolingian and Furongian Epochs in particular, experienced "supergreenhouse" climatic conditions. This term is used in a paleoclimate context to characterize geologic intervals of extraordinary warmth (Stephens et al., 2016). This in turn argues against glacio-eustatic fluctuations as drivers of repetitive facies transitions within the FMD. Under supergreenhouse conditions, orbitally driven fluctuations of sea level are thought to be minimal or completely absent (Catuneanu et al., 2009). We conclude, therefore, that conspicuous meter-scale alternations of peritidal facies seen in some portions of the FMD (Fig. 8) were primarily autocyclic and were not driven by glacio-eustatic sea-level change or other allocyclic forces.

Research on aquifer eustasy in epicratonic Cretaceous supergreenhouse settings suggests that geologically short-term shifts between humid to arid climate conditions can produce variations in aquifer charge and discharge that are volumetrically similar to the impact of waxing and waning glaciers (Hay and Leslie, 1990; Wendler and Wendler, 2016). Such variations can drive cyclic patterns in shallow carbonate systems (Wendler et al., 2016), and such patterns may occur in synchrony with Milankovitch- and sequence stratigraphic–scale cycles. In settings where geochronologic control is superb, it may be possible to link cyclic carbonate-hosted proxies like weathered clays to climate drivers and processes, such as increased chemical

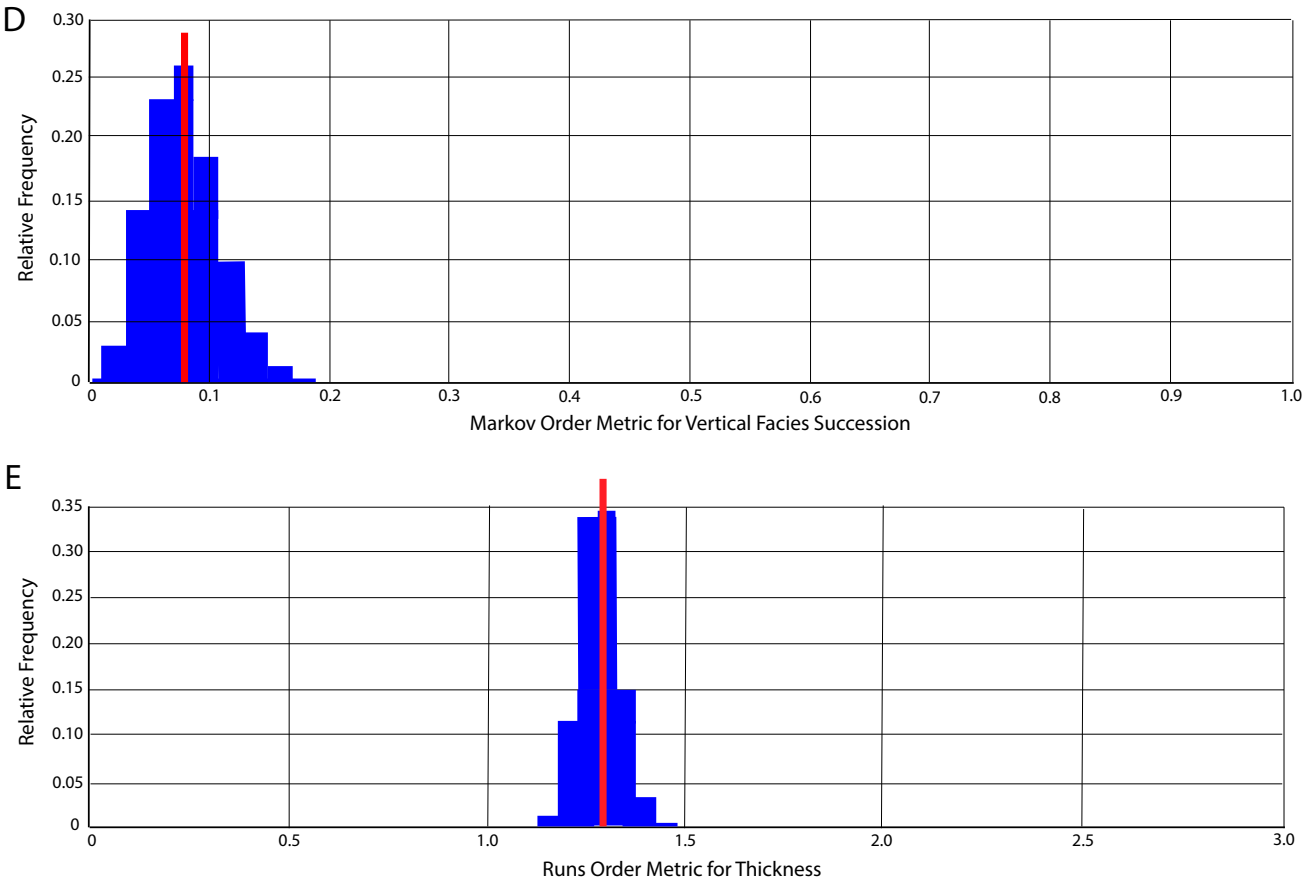

Figure 9 (*continued*). (D) Histogram of the Markov order metric (*m*). A value of 1 indicates a perfectly ordered data set; a value of 0 indicates a perfectly disordered data set. The red line indicates the observed value *m* = 0.081. The blue area shows the probability distribution of the metric based on 5000 random shuffles of the observed data. (E) Histogram of the runs order metric (*r*). The red line indicates the observed value *r* = 1.283. The blue area shows the probability distribution of the metric based on 5000 random shuffles of the observed data.

weathering under humid lowstand conditions, and vice versa (see reviews in Sames et al., 2020).

Examination of the FMD in craton-margin exposures typically involves hiking up narrow canyons or along narrow ridge crests. For that reason, it is difficult to trace the lateral continuity of individual beds, lithofacies, and stacking patterns. However, two studies of Furongian portions of the Great American Carbonate Bank in central Nevada and western Utah were specifically designed to test the lateral continuity of individual facies couplets (Zeiza, 2010; Widiarti, 2011). Both of these studies revealed that couplet boundaries disappear within tens to hundreds of meters parallel to bedding and that within individual couplets, the component facies pinch out or interfinger with other facies or with non-alternating intervals. In both cases, the researchers concluded that autocyclic processes, similar to those inherent in the aggrading-tidal-island model of Pratt and James (1986), were the agents responsible for the alternation of facies rather than allocyclic processes.

Autocyclic processes provide the simplest explanation for the succession of facies in the FMD. This conclusion is supported by our Markov order and runs order statistical analyses (Fig. 9). Aquifer-eustatic influences on these rocks are worth investigating through proxies such as weathering-sensitive minerals and derivative byproducts such as kaolinite and illite (e.g., Hallam et al., 1991; Bergaya et al., 2006).

THE STRATOTYPE AT FRENCHMAN MOUNTAIN

We establish a stratotype for the FMD at Frenchman Mountain that is accessible and on public land managed by the Bureau of Land Management (Fig. 10A). A detailed stratigraphic column, from Korolev (1997), is presented in Figure S1 (see footnote 1). The stratotype is located in a prominent unnamed canyon 0.7 km south of East Lake Mead Boulevard on the western face of the mountain (Figs. 10A and 11). The mouth of this canyon is at 36°11′29″ N, 115°0′28″ W. We define the base of the FMD in the stratotype as the sharp contact between dark gray, burrow-mottled, erosion-resistant dolostone of the Muav Formation and the overlying, light gray, less resistant dololaminite (Fig. 7). We define the top of the formation as the sharp contact between resistant, cliff-forming, reddish-weathering, glauconitic, bioclastic, echinoderm plate–rich grainstone and the overlying, brownish gray–weathering, ledge-forming, interbedded shale and dolostone of the Dunderberg Shale Member of the Nopah Formation (Fig. 7).

Accessing the FMD stratotype exposure requires bouldering skills, and the uppermost portion is very steep. Another exposure where

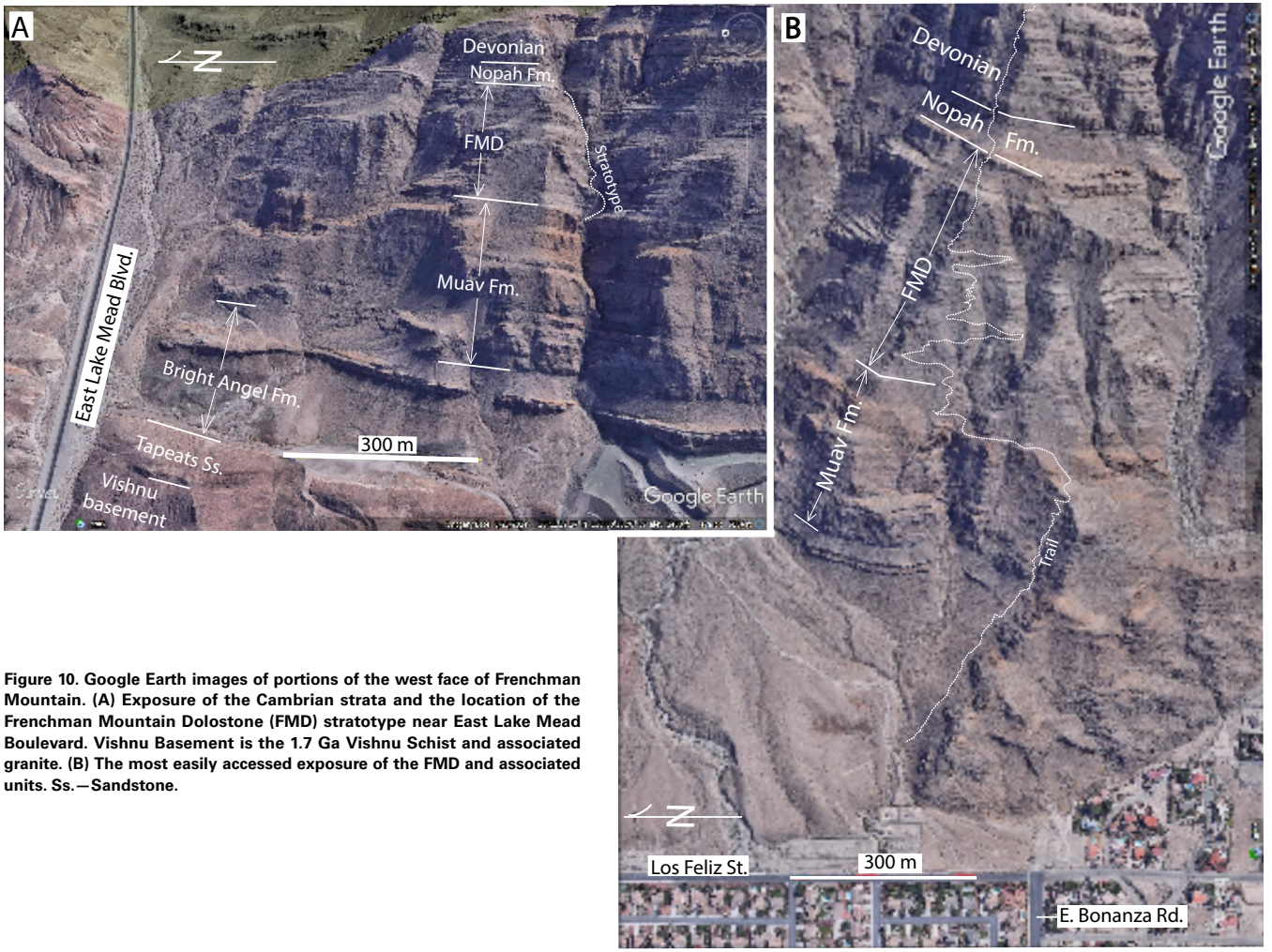

Figure 10. Google Earth images of portions of the west face of Frenchman Mountain. (A) Exposure of the Cambrian strata and the location of the Frenchman Mountain Dolostone (FMD) stratotype near East Lake Mead Boulevard. Vishnu Basement is the 1.7 Ga Vishnu Schist and associated granite. (B) The most easily accessed exposure of the FMD and associated units. Ss.—Sandstone.

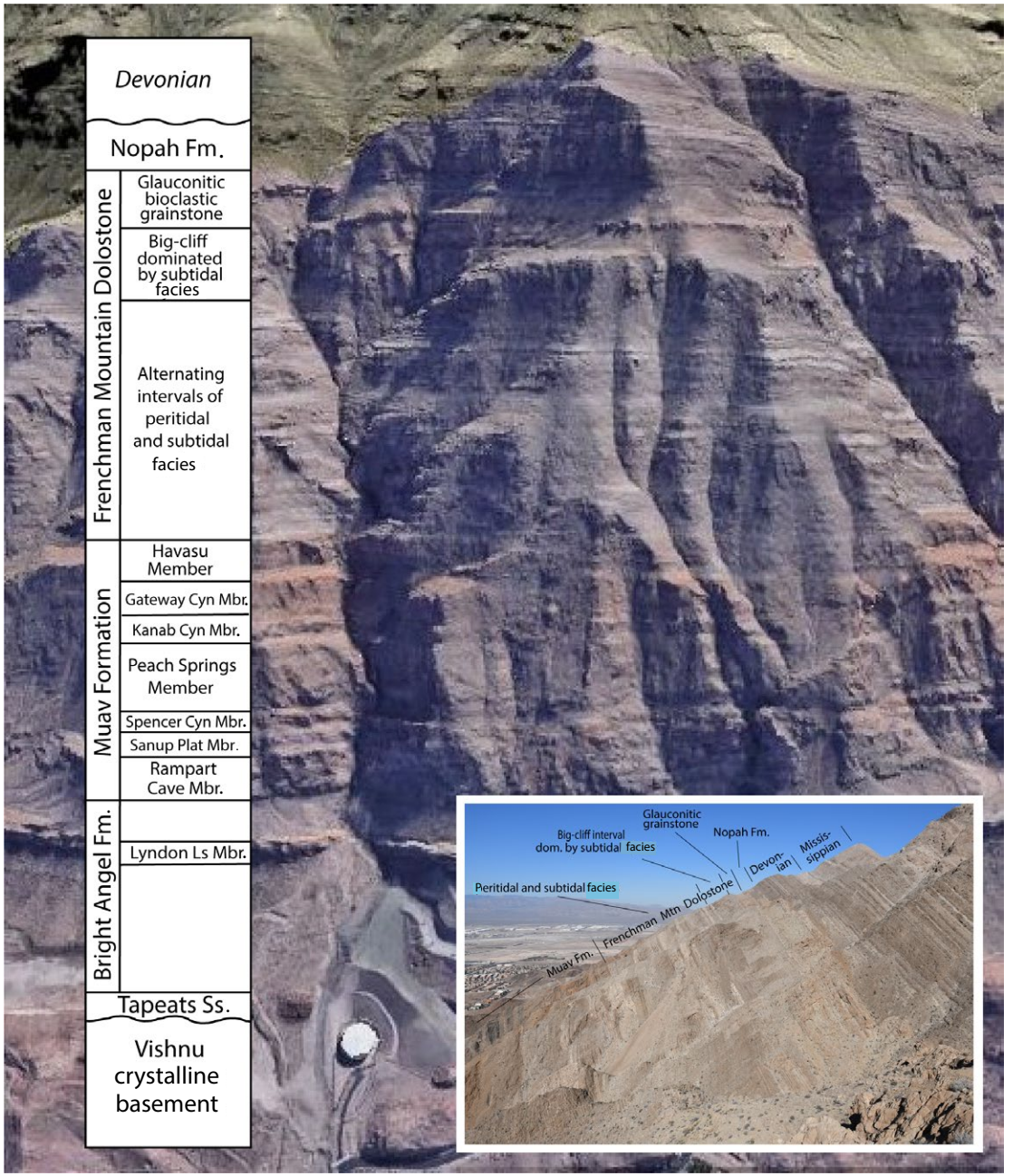

Figure 11. Google Earth image of the west face of Frenchman Mountain showing the entire Cambrian section as well as a portion of underlying crystalline basement rocks (consisting of the 1.7 GA Vishnu Schist and associated granite). The canyon left of center in this image contains the stratotype. Inset: Frenchman Mountain, looking north from the exposure east of East Bonanza Road. Ls—Limestone; Ss.—Sandstone.

the FMD and associated units may be more easily and safely examined is located 2 km to the south of the stratotype canyon, east of the intersection of East Bonanza Road and Los Feliz Street (Fig. 10B). There, a moderately steep, unmarked hiking trail, beginning at 36°10′33″ N, 115°0′54″ W, switches back and forth up the west face of the mountain through the Muav Formation, FMD, and overlying units. We measured the stratotype section prior to discovering the more easily accessible exposure.

Most of the stratotype lies on the Las Vegas NE 7.5′ quadrangle map, as does the more southerly exposure. The uppermost portion of the stratotype is on the Frenchman Mountain 7.5′ quadrangle map. Geologic maps of these quadrangles are available from the Nevada Bureau of Mines and Geology (Matti et al., 1993; Castor et al., 2000). The FMD was mapped as the Banded Mountain Member of the Bonanza King Formation by Matti et al. (1993) and as the Frenchman Mountain Dolomite by Castor et al. (2000). On the 1:100,000-scale Las Vegas 30′ × 60′ quadrangle geologic map (Page et al., 2004), it is mapped as Bonanza King Formation.

The complete Cambrian section at Frenchman Mountain is ~900 m thick (Rowland, 1987; Rowland et al., 1990), accounting for more than half of the strata exposed on the mountain's west face. Approximately half of the Cambrian section is composed of the 371-m-thick FMD, which is conformably overlain by the Furongian Nopah Formation. The Nopah Formation, which is 28 m thick at Frenchman Mountain (Sundberg, 1979), is disconformably overlain by the Devonian Mountain Springs Formation (Figs. 10, 11). This unit is disconformably overlain by 6.7 m of Middle Devonian strata of member C of the Mountain Springs Formation (Miller and Zilinsky, 1981). The Mountain Springs Formation is in turn overlain by the Devonian Sultan Limestone, which is correlative with the Temple Butte Formation in the Grand Canyon.

Biostratigraphy

The FMD has yielded no biostratigraphically useful fossils (McKee, 1945; Brathovde, 1986; Korolev, 1997; Middleton and Elliott, 2003). Microbialites and burrow-mottled dolomicrites are abundant, but these biosedimentary structures have no biostratigraphic value except when considered in an evolutionary or intrabasinal framework larger in scope than this study (e.g., Shapiro and Awramik, 2000).

In two of our measured sections in the Lake Mead region, the uppermost lithofacies of the FMD is a bioclastic grainstone composed of glauconite peloids, echinoderm plates, and rare trilobite spines seen only in thin section (Figs. 4, 6K, and 6L). None of these fossils are biostratigraphically diagnostic. Fossil assemblages employed to address the age of portions of the FMD have been described from bounding strata at Frenchman Mountain (Pack and Gayle, 1971; Palmer and Halley, 1979; Sundberg, 1979; Webster, 2011a) and correlative or bounding sections in Nevada at Sheep Mountain (Hardy, 1986), Muddy Mountains (Resser, 1945), Desert Range (Palmer, 1979; Fenton, 1980), Groom Range (Webster et al., 2011), and Split Mountain (Sundberg et al., 2011; Webster, 2011c; Lin et al., 2019).

The sedimentological analysis of the Bonanza King Formation by Montañez and Osleger (1993) included a Bonanza King section at Frenchman Mountain, the upper portion of which we now place within the FMD. Their determination that the Bonanza King Formation represents a fully aggraded, flat-topped carbonate platform permits the inference that the top of the FMD is correlative with the top of the Bonanza King, as depicted in Figure 12.

Fenton (1980) studied trilobites in a section of the Bonanza King Formation in the Desert Range, 65 km north-northwest of Frenchman Mountain. His study showed that the Papoose Lake Member lies at least partially within the *Glossopleura walcotti* Zone. The boundary between the *Glossopleura walcotti* Zone and the *Ehmaniella* Zone is poorly constrained in the Bonanza King Formation due to a dearth of trilobites; it occurs roughly in the middle of the Papoose Lake Member, which is reinforced by our chemostratigraphic data, discussed below.

Above the "silty interval," the Banded Mountain Member of the Bonanza King Formation contains *Ehmaniella* Zone taxa at its base, followed by *Bolaspidella*, *Cedaria*, and *Crepicephalus* Zone taxa, up to within ~10 m of the top (Fig. 12). In the Desert Range, Palmer (1979) documented trilobites that bracket the *Crepicephalus-Aphelaspis* Zone boundary up to 9 m below the top of the Bonanza King Formation. Similarly, Fenton (1980) recovered a diverse fauna of *Aphelaspis* Zone trilobites within the upper ten meters of the Bonanza King Formation, up to the top meter. He reported the first appearance of *Dicanthopyge*, marking the base of the *Dicanthopyge* Zone, in the top meter of this unit (Fig. 12).

Sundberg (1979) examined the biostratigraphy of the Dunderberg Shale and Halfpint Members of the Nopah Formation, which conformably overlies the Bonanza King Formation. He found no identifiable trilobites in Frenchman Mountain exposures; however, in other sections, he found *Dicanthopyge* Zone taxa within the lower few meters of the Dunderberg Shale, succeeded in turn by *Prehousia* Zone, *Dunderbergia* Zone, and *Elvinia* Zone taxa, as depicted in Figure 12. The presence of *Dicanthopyge* through *Elvinia* Zone fossils in the Dunderberg Shale and Halfpint Members of the Nopah Formation was also reported by Miller et al. (1981).

In sections examined in this study, we did not observe karstic features at the contact between the Frenchman Mountain Dolostone and the Dunderberg Shale. However, Keller et al., (2012) reported the common occurrence of such features at the top of the Bonanza King Formation in southern Great Basin exposures, recording emergence and exposure. Thus, we infer the presence of a depositional hiatus between the Frenchman Mountain Dolostone and the Nopah Formation (Fig. 12). This horizon defines the top of supersequence γ of Keller et al. (2012). Morgan (2012) and Taylor et al. (2012) used this same horizon to define the top of their Sauk II supersequence. The presence of *Dicanthopyge* Zone trilobites in the uppermost Bonanza King Formation and also in the base of the Dunderberg Shale (Fig. 12) suggests that this depositional hiatus was relatively brief.

The presence of Furongian Series trilobites, i.e., *Aphelaspis* Zone and *Dicanthopyge* Zone taxa, in the upper ten meters of the Bonanza King Formation documents that this formation, and therefore the FMD, extends across the Miaolingian-Furongian

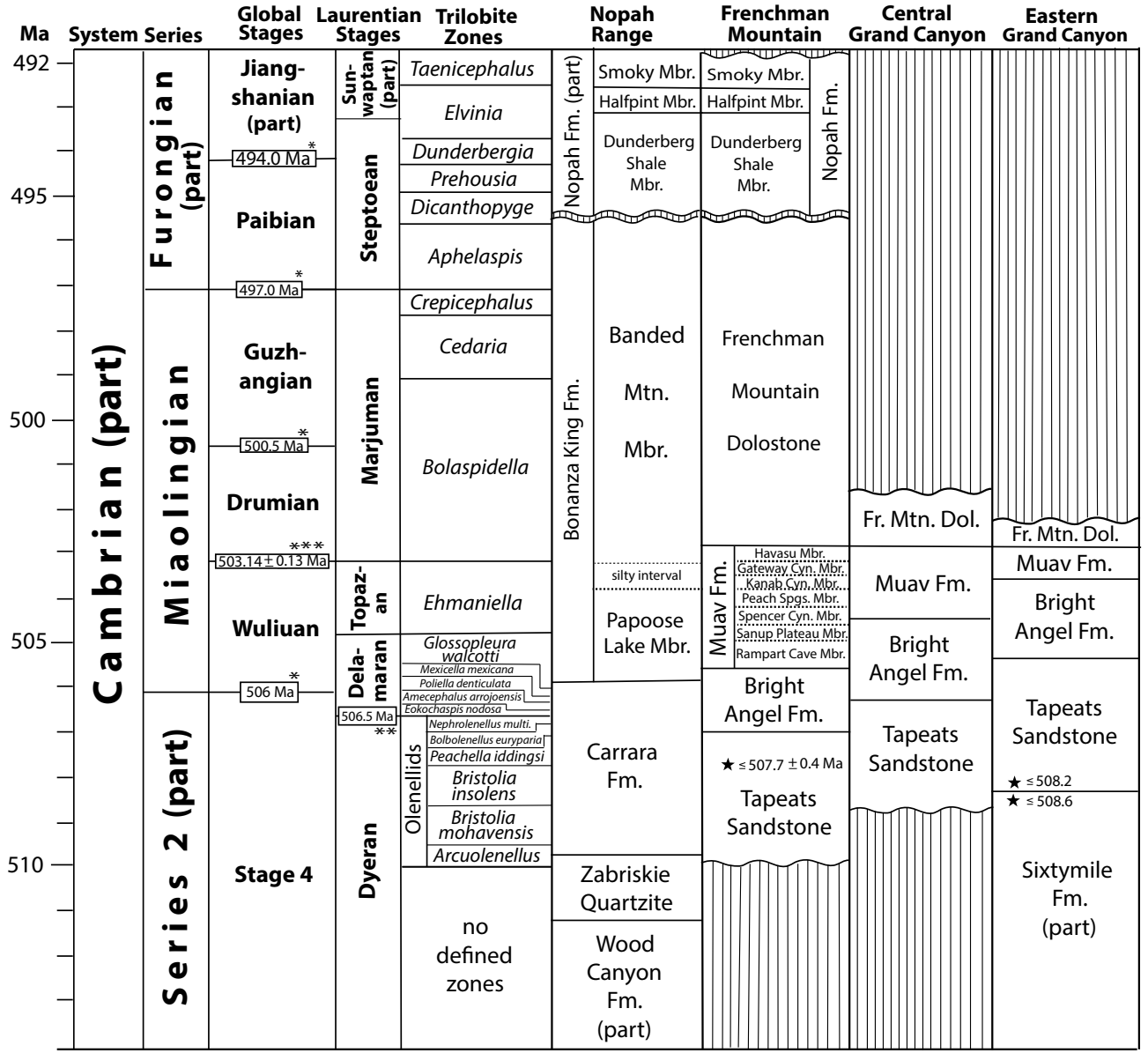

* Dates ±~0.5 m.y. (Peng et al., 2012)
** Date ≤ 0.5 m.y. (Karlstrom et al., 2020)
*** Landing et al. (2015); Sundberg et al. (2020)
★ U-Pb maximum depositional age from detrital zircons (Karlstrom et al., 2020)

Figure 12. Time-rock stratigraphic diagram and trilobite biostratigraphy of a portion of the Cambrian strata in the Grand Canyon (Arizona), at Frenchman Mountain (Nevada), and in the Nopah Range (California). Radiometric constraints on the Nopah Formation are from Morgan (2012). Biostratigraphic constraints on the Bright Angel Formation at Frenchman Mountain are from Webster (2011b), Karlstrom et al. (2020), and Sundberg et al. (2020); constraints on the Bright Angel Formation in the Grand Canyon are from McKee (1945), Resser (1945), Rose (2006), and Karlstrom et al. (2020). Biostratigraphic constraints on the Muav Formation in the Grand Canyon are from Rose (2011), McKee (1945), and Resser (1945). Biostratigraphic constraints on Bonanza King Formation are based on Palmer and Hazzard (1956) and Fenton (1980). Biostratigraphic constraints on the Carrara Formation are from Palmer and Halley (1979). cyn—canyon, dol—dolostone, spgs—springs, *multi.—multinodus*, Fr.—Frenchman.

boundary (Fig. 12; cf. Karlstrom et al., 2018, 2020; Sundberg et al., 2020).

$\delta^{13}C_{carb}$ Isotope Profile

In order to place the $\delta^{13}C_{carb}$ chemostratigraphy of the FMD into a global context, we sampled all Cambrian carbonates at Frenchman Mountain from the Lyndon Limestone Member of the Bright Angel Formation through the Nopah Formation (Fig. 13; Table S1, see footnote 1). This suite provides a preliminary regional reference section for Miaolingian-to-Furongian $\delta^{13}C_{carb}$ chemostratigraphy of the central Basin and Range and permits identification of global and within-basin isotopic patterns.

There are five notable chemostratigraphic features in the succession, including, from oldest to youngest, two Wuliuan negative excursions, an unconformity- or condensation-revealing isotopic shift at the Wuliuan-Drumian boundary, a Drumian negative excursion or couplet of excursions, and a large positive excursion in the Paibian (Steptoean). These five chemostratigraphic features are preceded by trends toward nadir and/or acme values, are not represented by lone data points, and have been reproduced by replicate sampling of excursion-bearing and excursion-bounding samples from the Frenchman Mountain succession.

The lowest of these excursions is recorded in the Lyndon Limestone Member of the Bright Angel Formation (N5? in Fig. 13). It is actually a pair of negative excursions, the lower of which descends to a nadir of –5‰, followed by a return to values near 0‰. The upper excursion then descends to –2.6‰. This pair of excursions spans ~15 m of section and corresponds biostratigraphically with the lower *Glossopleura walcotti* Zone. A coeval negative excursion was documented by Montañez et al. (2000) in the Papoose Lake Member of the Bonanza King Formation at Jangle Ridge, Nevada, and elsewhere. A negative excursion at approximately this stratigraphic level also occurs in the Emigrant Formation at Split Mountain, Nevada, where Lin et al. (2019) termed it the N5 excursion. This stratigraphic interval corresponds to the Tincanebits and Meriwitica Tongues of the Bright Angel Formation, two distinctive, ridge-forming Grand Canyon units (McKee, 1945). These two tongues amalgamate westward within the Grand Canyon to form the Lyndon Limestone at Frenchman Mountain and elsewhere in the southern Great Basin. Given the possibility that the tops of the Tincanebits and Meriwitica Tongues represent maximum flooding surfaces or sequence boundaries, a regional examination of this pattern and potential diagenetic linkages is merited.

The next prominent negative excursion, to –2.0‰, occurs in the basal Spencer Canyon Member of the Muav Formation. This excursion, labeled N6? in Figure 13, is not at the unit contact, but is stratigraphically within the transition from the *Glossopleura walcotti* Zone to the *Ehmaniella* Zone. This is similar to an excursion documented in the Banded Mountain Member of the Bonanza King Formation at Indian Ridge, Nevada (Montañez et al., 2000), and also in the Emigrant Formation at Split Mountain, where Lin et al. (2019) termed it the N6 excursion. The co-occurrence of these negative excursions with trilobite extinctions, i.e., zone boundaries, suggests a causal relation, at least within the southern Great Basin.

Higher in the succession, in the Gateway Canyon Member of the Muav Formation, there is a sharp change from negative-trending values to positive values at or close to the *Ehmaniella-Bolaspidella* Zone transition, which translates globally to the Wuliuan-Drumian Stage boundary (Fig. 13). This offset suggests that an unrecognized unconformity is present in the Gateway Canyon Member of the Muav Formation or that this represents a condensed interval not captured by our relatively coarse (1.5 m) sampling of this unit. This unconformity or condensed interval occurs near the top of the silty interval of the Muav Formation and Bonanza King Formation. We suggest that this surface corresponds to the regionally extensive sequence boundary and sub-Drumian Carbon Isotope Excursion (DICE) unconformity that Howley and Jiang (2010) documented throughout the Great Basin, including in the Banded Mountain Member of the Bonanza King Formation in the nearby Desert Range. It is very close to the global Wuliuan-Drumian boundary and is similar in age and magnitude to a ~4‰ negative shift documented by Shembilu and Azmy (2021) near the boundary between the Hawke Bay and March Point Formations in Newfoundland, Canada.

Stratigraphically higher, in the lower FMD, there is a robust trend toward negative $\delta^{13}C_{carb}$ values that is interpreted to occur in the lower *Bolaspidella* Zone. Like the possible N5 negative excursion in the Lyndon Limestone Member of the Bright Angel Formation, it is also a couplet of negative values, spanning ~18 m of strata. The lower nadir of the couplet is –2.7‰ and the upper nadir of the couplet is –2.5‰. We tentatively interpret this couplet to represent the global DICE event. Its interpreted position in the lower *Bolaspidella* Zone is internally consistent with documentation of the DICE in the basal portion of the Drumian Stage throughout the Great Basin (Brasier and Sukhov, 1998; Montañez et al., 2000; Babcock et al., 2007; Howley and Jiang, 2010). The proximity of these excursions to the unconformity at the Muav Formation–FMD contact suggests that this isotopic shift is associated with a change in environments, although there is no covariance in $\delta^{18}O$ values (R^2 = 0.04; Fig. S2, see footnote 1) that would suggest pervasive meteoric diagenesis.

Near the top of the Frenchman Mountain succession is the only conspicuous positive excursion (to 3.5‰). This event begins in the upper FMD and continues upward into the Dunderberg Shale and Halfpint Members of the Nopah Formation. The excursion spans ~28 m of strata, including six trilobite zones from the *Aphelaspis* to *Taenicephalus* Zones.

The $\delta^{13}C_{carb}$ chemostratigraphy of the FMD is best considered in the context of both local basin-scale Cambrian chemostratigraphy and emerging global Cambrian chemostratigraphic compilations (Zhu et al., 2004; Barili et al., 2018; Cramer and Jarvis, 2020). Overall, the chemostratigraphy of the succession exhibits a remarkably similar pattern to both global and local (i.e., Great Basin) chemostratigraphic records. There are five notable features in the succession, including, from oldest to youngest, the N5 and N6 negative excursions, an unconformity- or condensation-revealing isotopic shift at the Wuliuan-Drumian boundary, the DICE event, and the Steptoean Positive Carbon Isotope Excursion (SPICE) event.

The positive excursion (~3.5‰) that spans the uppermost FMD and the Nopah Formation is

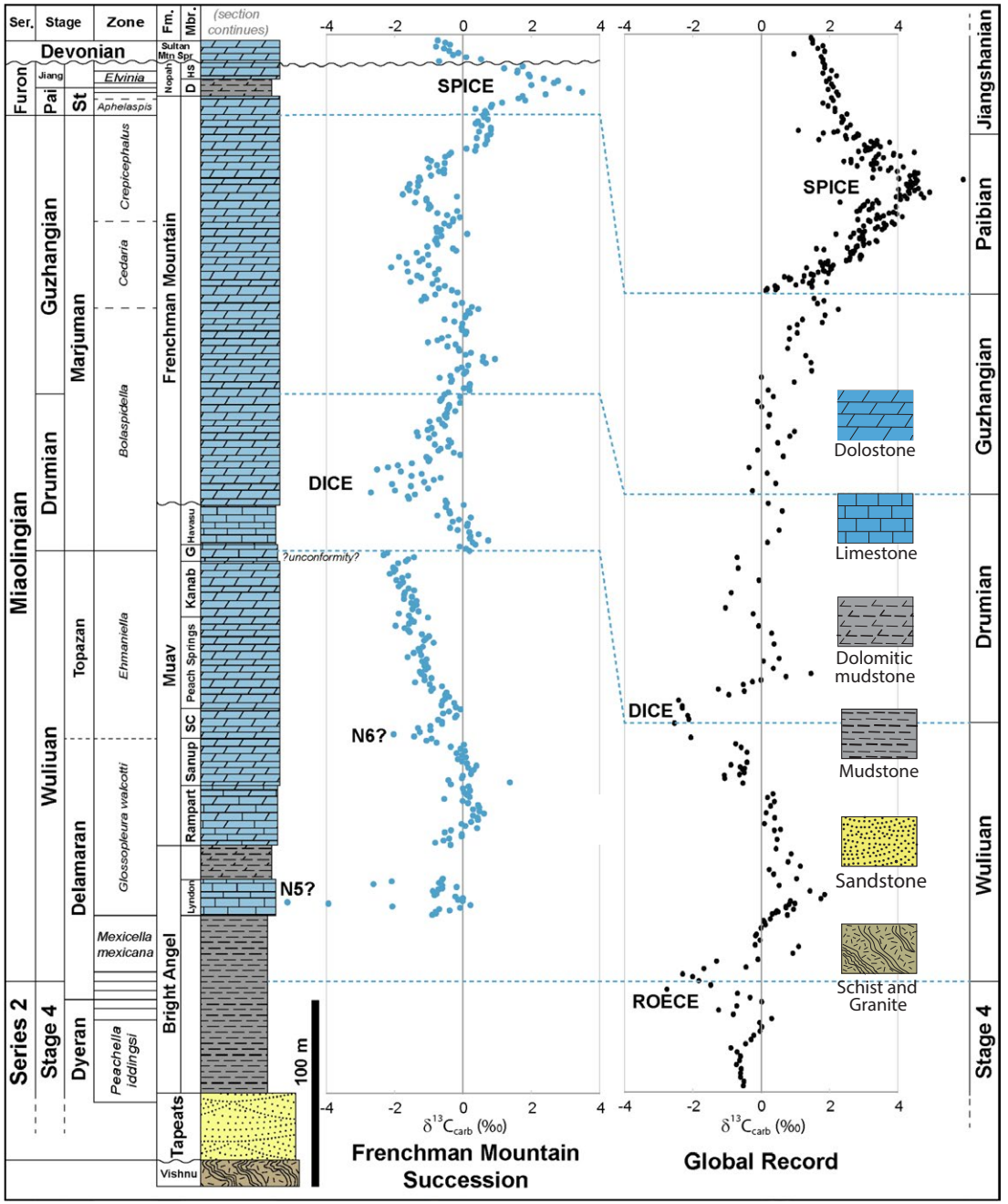

Figure 13. Chemostratigraphy and biostratigraphy of the Frenchman Mountain succession compared to the composite global reference curve. Durations of Cambrian stages at right are scaled linearly, whereas the Frenchman Mountain succession at left is scaled to rock thickness of the succession; the blue dashed lines indicate approximate tie points between stage boundaries and illustrate how excursions in the Frenchman Mountain section compare directly with global patterns. Key elements include the N5 and N6 excursions of Lin et al. (2019) in the upper Bright Angel and basal Muav Formations, respectively; a cryptic disconformity or condensed interval in the upper Muav; the global Drumian Carbon Isotope Excursion (DICE) at the base of the Frenchman Mountain Dolostone (FMD); and the Steptoean Positive Carbon Isotope Excursion (SPICE), which spans the FMD to Nopah Formation transition. Global curve at right is assembled from Chang et al. (2017), Saltzman et al. (2000), Zhu et al. (2004), and Peng et al. (2012), per Cramer and Jarvis (2020). Due to font size limitations, the trilobite zones between *Peachella iddingsi* and *Mexicella mexicana* and between *Aphelaspis* and *Elvinia* are not repeated from Figure 12. C_{carb} refers to stable carbon isotope ratios in marine carbonate rocks. ROECE—Redlichiid-Olenellid Extinction Carbon isotope Excursion; Lyndon—Lyndon Limestone; Rampart—Rampart Cave Member of Muav Formation; Sanup—Sanup Plateau Member of Muav Formation; SC—Spencer Canyon Member of Muav Formation; Peach Springs—Peach Springs Member of Muav Formation; Kanab—Kanab Canyon Member of Muav Formation; G—Gateway Canyon Member of Muav Limestone; Havasu—Havasu Member of Muav Formation; Vishnu—Vishnu Schist; Tapeats—Tapeats Sandstone; Bright Angel—Bright Angel Formation; Muav—Muav Formation; Frenchman Mountain—Frenchman Mountain Dolostone; Nopah—Nopah Formation; Mtn. Spr.—Mountain Springs Formation; Sultan—Sultan Limestone; D—Dunderberg Shale; HS—Halfpint and Smoky members; Furon—Furongian Series; St—Steptoean Stage; Pai—Paibian Stage; Jiang—Jiangshanian Stage; Ser.—series.

similar in stratigraphic position and magnitude to the global SPICE event identified by Saltzman et al. (1998, 2000) at Shingle Pass in east-central Nevada, and elsewhere in the Great Basin. We interpret this excursion in the Frenchman Mountain section as the SPICE event. Interestingly, although the *Elvinia* and *Taenicephalus* Zones are present in the Smoky Member of the Nopah Formation at Frenchman Mountain, the $\delta^{13}C$ values do not return to values between 0‰ and 1‰, as they do in SPICE-bearing successions at Shingle Pass, Nevada, and elsewhere in Laurentian basins (Saltzman et al., 2004). Perhaps this could be because the signal is condensed or telescoped at Frenchman Mountain because we did not sample at high enough resolution, or because the time-transgressive nature of this extinction within the Great Basin is poorly constrained (sensu Schiffbauer et al., 2017; Pulsipher et al., 2021; Shembilu and Azmy, 2021). If the SPICE is time transgressive in the southern Great Basin, it is possible that the trend away from the SPICE's isotopic zenith is truncated by the unconformity at the base of the Devonian Mountain Springs Formation. As a cautionary note, the Cambrian-Devonian disconformity is cryptic at Frenchman Mountain as well as in other Lake Mead–region sections. The chemostratigraphic trend with the Devonian Mountain Springs Formation and Sultan Limestone coincidentally reveals a negative trend that appears to be remarkably in line with the trending-toward-zero values of the underlying Nopah Formation. The conformance of this trend is particularly relevant for exposures to the east of Frenchman Mountain because they commonly lack clastics or pronounced lithologic changes that help visually define the unconformity in the field.

Finally, we acknowledge that our chemostratigraphy for this succession is preliminary and that postdepositional processes could be driving some of the signals in this record. For example, meteoric diagenesis can be a major driver of regional- and global-scale trends, particularly negative $\delta^{13}C$ excursions (see also Geyman and Maloof, 2019). Comparison of $\delta^{18}O$ to $\delta^{13}C$ for the Cambrian succession at Frenchman Mountain reveals no strong covariance ($R^2 = 0.44$) of values when all units are considered as a group (Fig. S2). Yet, cross-plotting of values within each member or unit reveals that certain stratigraphic intervals, especially the Lyndon Limestone (Bright Angel Formation; $R^2 = 0.67$), Rampart Cave (Muav Formation; $R^2 = 0.59$), Spencer Canyon (Muav Formation; $R^2 = 0.81$), and Dunderberg Shale (Nopah Formation; $R^2 = 0.71$) Members, exhibit notable covariance. Because the Lyndon Limestone, Rampart Cave, and Spencer Canyon Members are punctuated by the N5 and N6 excursions, higher-resolution sampling coupled with Mn/Sr analysis, cathodoluminescence, and trace element analysis (e.g., Shembilu and Azmy, 2021) would likely yield insightful results.

Despite these as-yet-unconstrained preservational and diagenetic risks, it is remarkable how similar the timing, scope, and magnitude of excursions in the $\delta^{13}C$ record of the Frenchman Mountain succession are to the global and regional $\delta^{13}C$ records cited. This similarity suggests that the section is at least recording global to regional changes in carbon cycling.

AN AGE MODEL FOR THE TONTO GROUP

Integration of biostratigraphic, chemostratigraphic, and sequence stratigraphic data for the Frenchman Mountain Dolostone along with chemostratigraphic, biostratigraphic, and U-Pb-based geochronologic data from the rest of the Cambrian succession (Karlstrom et al., 2020) and the global syntheses of Peng et al. (2012, 2020) permits us to propose a working-hypothesis age model for the Tonto Group at Frenchman Mountain, as summarized in Figure 12. This age model will be tested and modified as new dates are obtained and fossils discovered.

Starting at the base of the succession at Frenchman Mountain, the age of the Tapeats Sandstone, which contains no body fossils, remains poorly constrained. Karlstrom et al. (2020) reported a U-Pb chemical abrasion–isotope dilution thermal ionization mass spectrometry (CA-IDTIMS) maximum-depositional age (MDA) of 507.7 Ma on detrital zircon for a sample collected ~30 m above the base of the Tapeats at Frenchman Mountain (Matthews et al. 2018), where this formation is 48 m thick (Rowland et al., 1990). An MDA of 508.2 Ma was also determined for a sample collected near the base of the Tapeats in the eastern Grand Canyon (Karlstrom et al., 2020). Based on these ages, Karlstrom et al. (2020) concluded that the Tapeats Sandstone was deposited within a two-million-year interval, ca. 508–507 Ma. We tentatively place the base of the Tapeats Sandstone at Frenchman Mountain closer to 510 Ma, based primarily on the supposition that it is correlative in part with the Zabriskie Quartzite of the Death Valley, California, region (Fig. 12). The geochronologic age of the top of the Zabriskie is not tightly constrained, but it is biostratigraphically constrained by trilobites in the overlying Carrara Formation (Palmer and Halley, 1979) (Fig. 12).

Dyeran trilobite biostratigraphy within the Bright Angel Formation at Frenchman Mountain has been investigated by Webster (2011a, 2011b). As reflected in Figure 12, the lowest trilobites in this section are olenellids of the *Peachella iddingsi* Zone (Webster 2011a; see also Sundberg et al., 2020; Foster, 2021; Rowland, 2022). These are overlain by olenellids of the *Bolbolenellus euryparia* and *Nephrolenellus multinodus* Zones, respectively. The top of the *N. multinodus* Zone marks the extinction of olenellids, which also traditionally defines the top of the Dyeran Stage. At Frenchman Mountain, this boundary lies ~25 m above the base of the Bright Angel Formation (Webster, 2011b; Sundberg et al., 2020; Rowland, 2022). In Laurentia, this horizon is dated at ca. 506.5 Ma (Sundberg et al., 2020) (Fig. 12). The age of the base of the Bright Angel Formation is not tightly constrained, but it must be older than 506.5 Ma and younger than 507.7 Ma, the MDA of detrital zircons in the Tapeats Sandstone (Fig. 12). We tentatively place the age of the base of the Bright Angel Formation at Frenchman Mountain at ca. 506.7 Ma and the age of the Bright Angel Formation–Muav Formation contact at ca. 505.5 Ma (see below). This implies that the Bright Angel Formation was deposited over a relatively brief interval of ~1.2 m.y. This interval will be better constrained with future work.

Our results indicate that the Muav Formation does not span as much time as previously proposed. Assignment of the basal contact of the Muav

to the base of the *Ehmaniella* Zone, as proposed by Karlstrom et al. (2020), cannot be reconciled with new data; such placement is too young, at least for Frenchman Mountain and western Grand Canyon exposures. The lowest two units of the Muav, the Rampart Cave and Sanup Plateau Members, lie within the *Glossopleura walcotti* Zone in Peach Springs Canyon of the western Grand Canyon (Sundberg, 2011) and presumably also at Frenchman Mountain. Rose (2011) suggested that this zone might extend as high as the Peach Springs Member of the Muav; however, the biostratigraphy and chemostratigraphy presented here and also by Lin et al. (2019) require placement of the upper limit of this zone lower in the succession (at excursion N6 in Fig. 13), at least in the Frenchman Mountain and western Grand Canyon sections. We recognize that the base of the Muav Formation probably becomes younger toward the east, as does the underlying Bright Angel Formation—hypotheses internally consistent with our data and with data from McKee (1945), Resser (1945), and subsequent authors (e.g., Karlstrom et al., 2018, 2020).

Moving stratigraphically higher in the Muav, a shale horizon at the top of the Peach Springs Member in some Grand Canyon exposures contains specimens of the trilobite *Glyphaspis*, which is an *Ehmaniella* Zone taxon (Rose, 2011). *Glyphaspis* also occurs in the Gateway Canyon Member (McKee, 1945). Sundberg (2011) reported the occurrence of upper *Ehmaniella* Zone trilobites in the Gateway Canyon Member in Peach Springs Canyon. Such fossil occurrences are internally consistent with extension of the *Ehmaniella* Zone well up into the Gateway Canyon Member to the first appearance of bolaspidellid trilobites (McKee, 1945).

We hypothesize that the *Ehmaniella-Bolaspidella* Zone boundary occurs at our observed chemostratigraphic truncation of the global terminal-Wuliuan negative $\delta^{13}C$ trend within the Gateway Canyon Member, toward the top of the "silty interval" (Fig. 13). We further hypothesize that this boundary also coincides with the regional unconformity identified by Howley and Jiang (2010).

The Havasu Member—the uppermost member of the Muav—has not yet yielded fossils. We conservatively interpret this member to lie within the lower portion of the *Bolaspidella* Zone (Figs. 12 and 13), an interpretation consistent with the biostratigraphy and chemostratigraphy of coeval strata in the southern and eastern Great Basin, including the silty interval (Howley and Jiang, 2010; this study).

The top of the Muav Formation is also older than previously hypothesized. Karlstrom et al. (2020) proposed that the Havasu Member lies within the *Cedaria* Zone, high in the Marjuman Stage, based on the presence of the trilobite *Spencella* (formerly *Solenopleurella*), which occurs several meters below the bottom of the Havasu Member. *Spencella* may possibly range into the *Bolaspidella* Zone, but it is primarily an *Ehmaniella* Zone taxon (Sundberg, 1991). Thus, there is no compelling biostratigraphic evidence to support the placement of the top of the Muav within the *Cedaria* Zone, nor do the chemostratigraphic data support such a placement. We suggest that the top of the Muav Formation occurs near the bottom of the *Bolaspidella* Zone (Fig. 12). This placement is based on our interpretation of the age of the FMD, the correlation of the "silty interval" and its capping unconformity throughout the Great Basin, and the presence of the DICE in the basal potion of the FMD.

Our age model suggests that the base of the Muav Formation is ca. 505.5 Ma, low in the Wuliuan Stage, while the age of its top is ca. 502.8 Ma, low in the Drumian Stage (Fig. 12). Thus the Muav Formation is hypothesized to represent ~2.7 m.y. of deposition.

Based primarily on the chemostratigraphic record, including the DICE, we infer the base of the FMD at Frenchman Mountain to be ca. 502.8 Ma, with its top at ca. 495.5 Ma (Fig. 12). Thus, the FMD was deposited over an interval of ~7.3 m.y.

Our age model suggests that the interval of the Tonto Group represented at Frenchman Mountain was deposited over a time interval spanning between 14 and 15 m.y. The FMD (along with the correlative Banded Mountain Member of the Bonanza King Formation) represents the waning stage of Sauk II—the second of the three commonly recognized phases of the Sauk Transgression.

Figure 14 shows time-thickness bar graphs (cf. Mayer and Dickinson, 1984) and net sediment accumulation rates for the formations of the Tonto

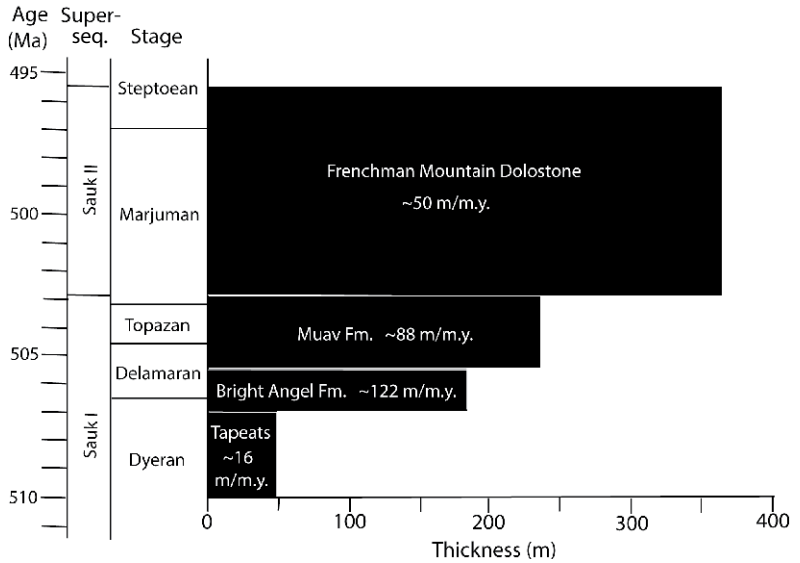

Figure 14. Time-thickness bar graphs for the formations of the Tonto Group at Frenchman Mountain, showing net sediment accumulation rates. Superseq.—Supersequence.

Group at Frenchman Mountain, based on the ages indicated in our age model. As indicated on these graphs, the Tapeats Sandstone has by far the lowest net sediment accumulation rate within this suite of formations, ~16 m/m.y. The rate increases dramatically upsection into the Bright Angel Formation; at ~122 m/m.y., this formation has the highest rate of net sediment accumulation within the Tonto Group. This is a minimum rate, however, because compaction of the fine-grained siliciclastic sediments in this unit was not taken into account and within-unit unconformities cannot be constrained. The rate of net sediment accumulation progressively decreased during deposition of the Tonto Group; the rate for the Muav Formation is ~88 m/m.y., while the rate for the FMD is ~50 m/m.y.

The 50 m/m.y. sediment accumulation rate for the FMD at Frenchman Mountain records a relatively low rate of net accumulation, which we interpret as representing the rate of passive-margin subsidence. Carbonate platforms commonly grow at rates of 100 m/m.y. and above (Schwab, 1976; Bosscher and Schlager, 1993). Cook and Taylor (1977) reported a sediment accumulation rate of 80 m/m.y. in the Miaolingian Whipple Cave Formation carbonate platform, ~200 km north of Frenchman Mountain. A slightly older (Terreneuvian to Miaolingian) carbonate platform in the Canadian Rockies accumulated sediment at a rate of 80 m/m.y. (Bond and Kominz, 1984).

CONCLUSIONS AND SUGGESTIONS FOR FURTHER RESEARCH

In 1945, Eddie McKee distinguished—but did not formally name—a cliff-forming interval of carbonate rocks of uncertain age overlying the Muav Formation in the Grand Canyon. After more than three-quarters of a century of obscurity and anonymity, these strata finally have a formally recognized name, a stratotype section, an age model constrained by litho-, bio-, and chemostratigraphy, a depositional environmental framework, and a stratigraphic connection with global events that were occurring half a billion years ago. The FMD is the capping formation of the Tonto Group. It was deposited in equatorial latitudes as a flat-topped, fully aggraded carbonate platform on the margin of the Laurentian craton, inboard of the "Great American Carbonate Bank." It is constructed of shallow-subtidal and peritidal facies. It is 371 m thick at its Frenchman Mountain stratotype locality, and it thins dramatically eastward into the Grand Canyon, largely due to pre–Middle Devonian erosion. Although meter-scale couplets of dark- and light-colored facies are visually conspicuous in portions of the formation, statistical analysis of the succession of facies and their thicknesses in the stratotype section provide no evidence of cyclicity or other forms of order. Autocyclic processes provide the simplest explanation for the succession of facies in this formation. The FMD spans ~7.3 m.y. of Miaolingian and Furongian time, including portions of five trilobite zones. It is correlative with all but the lower 130 m of the Banded Mountain Member of the Bonanza King Formation, one of the thickest and most recognizable rock formations in the southern Basin and Range province.

The relative ease of access, thickness, and unvegetated exposure of the FMD at Frenchman Mountain and other Lake Mead–region sites offers diverse opportunities for future research. For example, the unit is ripe for higher-spatial-resolution $\delta^{13}C_{carb}$ chemostratigraphic or trace element analysis of the DICE, $^{87}Sr/^{86}Sr$ chemostratigraphic analysis to assess the regional position of the Drumian-Guzhangian boundary, and magnetic susceptibility or clay analyses of cyclic facies to reconstruct a Cambrian aridity-humidity record. Similarly, correlation and geochronologic hypotheses presented herein would benefit from an array of biostratigraphic and geochronologic work, such as a targeted search for identifiable trilobite fragments in the bioclastic grainstones, dissolution of samples for phosphatic microfossils, and maximum depositional age–focused U-Pb analysis of windblown detrital grains throughout the FMD's siltier intervals.

The Frenchman Mountain exposure of the FMD provides a felicitous opportunity for more rigorously pursuing the question of the generation of meter-scale and sub-meter-scale cyclicity on carbonate platforms. Meter-scale and sub-meter-scale rhythmic alternations of facies are well exposed and accessible.

Sub-FMD units within the Frenchman Mountain section also contain signals of potentially regional or global significance that merit further scrutiny. For example, the cryptic unconformity and $\delta^{13}C_{carb}$ excursions (N5, N6) in the Muav and Bright Angel Formations that we identified are hypothesized to be tied to trilobite extinctions and/or regional flooding or exposure events as represented by the Lyndon Limestone Member, Tincanebits Tongue, and Meriwitica Tongue of the Bright Angel. Such hypotheses are testable through focused, high-resolution chemostratigraphy and biostratigraphy of cratonic and basinal exposures of these intervals.

ACKNOWLEDGMENTS

We gratefully acknowledge financial support from patrons of the Denver Museum of Nature and Science, the University of Nevada Las Vegas (UNLV) paleontological research fund, the David B. Jones Foundation, and U.S. National Science Foundation (NSF) grant EAR-1954634. Korolev acknowledges the UNLV Graduate and Professional Student Association. Thanks to F. Bachhuber for the use of his motorized canoe. K. Karlstrom and L. Crossey provided critical logistical support and useful discussions regarding Cambrian stratigraphic nomenclature. Grand Canyon fieldwork in 2019 was conducted under research permits of K. Karlstrom with Grand Canyon National Park. Frenchman Mountain samples for chemostratigraphic analysis were collected under Bureau of Land Management (BLM) research permit N-100230 to Rowland. M. Holland, C. Dehler, and students assisted in the measurement of sections in the eastern and central Grand Canyon and with stratigraphic and chemostratigraphic interpretations. F. Sundberg provided suggestions regarding biostratigraphy and the construction of Figures 12 and 13, and R. Metcalf assisted with photomicrographs. D. Dettman and the team at the University of Arizona's Environmental Isotope Laboratory are thanked for their assistance with geochemical analyses. K. Azmy, F. Corsetti, C. Dehler, G. Jiang, K. Karlstrom, and B. Pratt provided helpful reviews of an early draft. Thanks to reviewers Galen Halverson and Bruce Wilkinson, Associate Editor Greg Hoke, and Science Editor David Fastovsky for insightful reviews that helped improve this paper.

REFERENCES CITED

Assereto, R.L.A.M., and Kendall, C.G.St.C., 1977, Nature, origin, and classification of peritidal tepee structures and related breccias: Sedimentology, v. 24, p. 153–210, https://doi.org/10.1111/j.1365-3091.1977.tb00254.x.

Babcock, L.E., Robinson, R.A., Rees, M.N., Peng, S.C., and Saltzman, M.R., 2007, The Global boundary Stratotype Section and Point (GSSP) of the Drumian Stage (Cambrian) in the Drum Mountains, Utah, USA: Episodes, v. 30, p. 84–94.

Barili, R., Neilson, J.E., Brasier, A.T., Goldberg, K., Bardola, T.P., De Ros, L.F., and Leng, M., 2018, Carbon isotopes, stratigraphy, and environmental change: The Middle–Upper Cambrian Positive Excursion (SPICE) in Port au Port Group, western Newfoundland, Canada: Canadian Journal of Earth Sciences, v. 55, p. 1209–1222, https://doi.org/10.1139/cjes-2018-0025.

Barnaby, R.J., and Read, J.F., 1990, Carbonate ramp to rimmed shelf evolution: Lower to Middle Cambrian continental margin, Virginia Appalachians: Geological Society of America Bulletin, v. 102, p. 391–404, https://doi.org/10.1130/0016-7606(1990)102<0391:CRTRSE>2.3.CO;2.

Barnes, H., and Palmer, A.R., 1961, Revision of stratigraphic nomenclature of Cambrian rocks, Nevada Test Site and vicinity, Nevada, *in* Geological Survey Research 1961: Short Papers in the Geologic and Hydrologic Sciences, Articles 147–292: U.S. Geological Survey Professional Paper 424-C, p. 100–103.

Bathurst, R.G.C., 1972, Carbonate Sediments and their Diagenesis (2nd edition): Amsterdam, Elsevier, 658 p.

Bergaya, F., Theng, B.K.G., and Lagaly, G., eds., 2006, Handbook of Clay Science: Amsterdam, Elsevier, 1248 p.

Berner, R.A., and Kothavala, Z., 2001, GEOCARB III: A revised model of atmospheric CO_2 over Phanerozoic time: American Journal of Science, v. 301, p. 182–204, https://doi.org/10.2475/ajs.301.2.182.

Beus, S.S., and Morales, M., 2003, Introducing the Grand Canyon, *in* Beus, S.S., and Morales, M., eds., Grand Canyon Geology (2nd edition): New York, Oxford University Press, p. 1–8.

Blakey, R.C., and Middleton, L.T., 2012, Geologic history and paleogeography of Paleozoic and early Mesozoic sedimentary rocks, eastern Grand Canyon, *in* Timmons, J.M., and Karlstrom, K.E., eds., Grand Canyon Geology: Two Billion Years of Earth's History: Geological Society of America Special Paper 489, p. 81–92, https://doi.org/10.1130/2012.2489(05).

Bond, G.C., and Kominz, M.A., 1984, Construction of tectonic subsidence curves for the Early Paleozoic miogeocline, southern Canadian Rocky Mountains: Implications for subsidence mechanisms, age of breakup, and crustal thinning: Geological Society of America Bulletin, v. 95, p. 155–173, https://doi.org/10.1130/0016-7606(1984)95<155:COTSCF>2.0.CO;2.

Bosscher, H., and Schlager, W., 1993, Accumulation rates of carbonate platforms: The Journal of Geology, v. 101, p. 345–355, https://doi.org/10.1086/648228.

Brasier, M.D., and Sukhov, S.S., 1998, The falling amplitude of carbon isotope oscillations through the Lower to Middle Cambrian: Northern Siberian data: Canadian Journal of Earth Sciences, v. 35, p. 353–373, https://doi.org/10.1139/e97-122.

Brathovde, J.E., 1986, Stratigraphy of the Grand Wash Dolomite (Upper? Cambrian), western Grand Canyon, Mohave County, Arizona [M.S. thesis]: Flagstaff, Northern Arizona University, 140 p.

Burgess, P.M., 2006, The signal and the noise: Forward modeling of allocyclic and autocyclic processes influencing peritidal carbonate stacking patterns: Journal of Sedimentary Research, v. 76, p. 962–977, https://doi.org/10.2110/jsr.2006.084.

Burgess, P.M., 2008, The nature of shallow-water carbonate lithofacies thickness distributions: Geology, v. 36, p. 235–238, https://doi.org/10.1130/G243326A.1.

Burgess, P.M., 2016, Identifying ordered strata: Evidence, methods, and meaning: Journal of Sedimentary Research, v. 86, p. 148–167, https://doi.org/10.2110/jsr.2016.10.

Burne, R.V., and Moore, L.S., 1987, Microbialites: Organosedimentary deposits of benthic microbial communities: Palaios, v. 2, p. 241–254, https://doi.org/10.2307/3514674.

Castor, S.B., Faulds, J.E., Rowland, S.M., and dePolo, C.M., 2000, Geologic map of the Frenchman Mountain quadrangle, Clark County, Nevada: Nevada Bureau of Mines and Geology Map 127, scale 1:24,000.

Catuneanu, O., Abreu, V., Bhattacharya, J.P., Blum, M.D., Dalrymple, R.W., Eriksson, P.G., Fielding, C.R., Fisher, W.L., Galloway, W.E., Gibling, M.R., Giles, K.A., Holbrook, J.M., Jordan, R., Kendall, C.G.St.C., Macurda, B., Martinsen, O.J., Miall, A.D., Neal, J.E., Nummedal, D., Pomar, L., Posamentier, H.W., Pratt, B.R., Sarg, J.F., Shanley, K.W., Steel, R.J., Strasser, A., Tucker, M.E., and Winker, C., 2009, Towards the standardization of sequence stratigraphy: Earth-Science Reviews, v. 92, p. 1–33, https://doi.org/10.1016/j.earscirev.2008.10.003.

Chafetz, H.S., and Reid, A., 2000, Syndepositional shallow-water precipitation of glauconitic minerals: Sedimentary Geology, v. 136, p. 29–42, https://doi.org/10.1016/S0037-0738(00)00082-8.

Chang, C., Hu, W.X., Wang, X.L., Yu, H., Yang, A.H., Cao, J., and Yao, S.P., 2017, Carbon isotope stratigraphy of the lower to middle Cambrian of the eastern Yangtze Platform, South China: Palaeogeography, Palaeoclimatology, Palaeoecology, v. 479, p. 90–101, https://doi.org/10.1016/j.palaeo.2017.04.019.

Chaudhuri, A.K., 2005, Climbing ripple structure and associated storm-lamination from a Proterozoic carbonate platform succession: Their environmental and petrogenetic significance: Journal of Earth System Science, v. 114, p. 199–209, https://doi.org/10.1007/BF02702945.

Cloud, P.E., Jr., 1955, Physical limits of glauconite formation: American Association of Petroleum Geologists Bulletin, v. 39, p. 484–492, https://doi.org/10.1306/5CEAE166-16BB-11D7-8645000102C1865D.

Cook, H.E., and Taylor, M.E., 1977, Comparison of continental slope and shelf environments in the Upper Cambrian and lowest Ordovician of Nevada, *in* Cook, H.E., and Enos, P., eds., Deep-Water Carbonate Environments: Society of Economic Paleontologists and Mineralogists Special Publication 25, p. 51–81, https://doi.org/10.2110/pec.77.25.0051.

Cramer, B.D., and Jarvis, J., 2020, Carbon isotope stratigraphy, *in* Gradstein, F.M., Ogg, J.G., Schmitz, M.D., and Ogg, G.M., eds., Geologic Time Scale 2020: Amsterdam, Elsevier, p. 309–343, https://doi.org/10.1016/B978-0-12-824360-2.00011-5.

Dunham, R.J., 1962, Classification of carbonate rocks according to depositional texture, *in* Ham, W.E., ed., Classification of Carbonate Rocks—A Symposium: American Association of Petroleum Geologists Memoir 1, p. 108–121.

Dyer, B., and Maloof, A.C., 2015, Physical and chemical stratigraphy suggest small or absent glacioeustatic variation during formation of the Paradox Basin cyclothems: Earth and Planetary Science Letters, v. 419, p. 63–70, https://doi.org/10.1016/j.epsl.2015.03.017.

El Albani, A., Meunier, A., and Fürsich, F., 2005, Unusual occurrence of glauconite in a shallow lagoonal environment (Lower Cretaceous, northern Aquitaine Basin, SW France): Terra Nova, v. 17, p. 537–544, https://doi.org/10.1111/j.1365-3121.2005.00646.x.

Elston, D.P., 1989, Grand Canyon Supergroup, northern Arizona: Stratigraphic summary and preliminary paleomagnetic correlations with parts of other North American Proterozoic successions, *in* Jenney, J.P., and Reynolds, S.J., eds., Geologic Evolution of Arizona: Arizona Geological Society Digest 17, p. 259–272.

Fenton, S.B., 1980, Geology of the Bonanza King Formation (Cambrian) at the Desert Range, Clark County, Nevada [M.S. thesis]: San Diego, California, San Diego State University, 154 p.

Foster, J.R., 2021, Comparative trilobite taphonomy from the craton to the outer shelf, latest early Cambrian (Stage 4; late Dyeran) of the southern Great Basin, *in* Lucas, S.G., Hunt, A.P., and Lichtig, A.J., eds., Fossil Record 7: New Mexico Museum of Natural History and Science Bulletin 82, p. 75–92.

Fritz, R.D., Morgan, W.A., Longacre, S., Derby, J.R., and Sternbach, C.A., 2012, Introduction, *in* Derby, J., Fritz, R., Longacre, S., Morgan, W., and Sternbach, C., eds., The Great American Carbonate Bank: The Geology and Economic Resources of the Cambrian–Ordovician Sauk Megasequence of Laurentia: American Association of Petroleum Geologists Memoir 98, p. 1–3, https://doi.org/10.1306/13331486M980077.

Fryxell, J.E., and Deubendorfer, E.M., 2005, Origin and trajectory of the Frenchman Mountain block, an extensional allochthon in the Basin and Range province, southern Nevada: The Journal of Geology, v. 113, p. 355–371, https://doi.org/10.1086/428810.

Gans, W.T., 1974, Correlation and redefinition of the Goodsprings Dolomite, southern Nevada and eastern California: Geological Society of America Bulletin, v. 85, p. 189–200, https://doi.org/10.1130/0016-7606(1974)85<189:CAROTG>2.0.CO;2.

Garside, L.J., House, P.K., Burchfiel, B.C., Rowland, S.M., and Buck, B.J., 2012, Geologic map of the Jean quadrangle, Clark County, Nevada: Nevada Bureau of Mines and Geology Map 176, scale 1:24,000.

Geyman, E.C., and Maloof, A.C., 2019, A diurnal carbon engine explains ^{13}C-enriched carbonates without increasing the global production of oxygen: Proceedings of the National Academy of Sciences of the United States of America, v. 116, p. 24,433–24,439, https://doi.org/10.1073/pnas.1908783116.

Gilbert, G.K., 1875, Report on the geology of portions of Nevada, Utah, California, and Arizona, *in* Report upon Geographical and Geological Explorations and Surveys West of the One Hundredth Meridian: Washington, D.C., U.S. Government Printing Office, v. 3, Part 1, p. 17–187.

Guo, C., Chen, D.Z., Song, Y.F., Zhou, X.Q., Ding, Y., and Zhang, G.J., 2018a, Depositional environments and cyclicity of the Early Ordovician carbonate ramp in the western Tarim Basin (NW China): Journal of Asian Earth Sciences, v. 158, p. 29–48, https://doi.org/10.1016/j.jseaes.2018.02.006.

Guo, C., Chen, D.Z., Zhou, X.Q., Ding, Y., Wei, W.W., and Zhang, G.J., 2018b, Depositional facies and cyclic patterns in a subtidal-dominated ramp during the Early-Middle Ordovician in the western Tarim Basin (NW China): Facies, v. 64, 16, https://doi.org/10.1007/s10347-018-0529-0.

Hallam, A., Grose, J.A., and Ruffell, A.H., 1991, Paleoclimatic significance of changes in clay mineralogy across the

Jurassic-Cretaceous boundary in England and France: Palaeogeography, Palaeoclimatology, Palaeoecology, v. 81, p. 173–187, https://doi.org/10.1016/0031-0182(91)90146-I.

Hardy, J.K., 1986, Stratigraphy and depositional environments of Lower and Middle Cambrian strata in the Lake Mead region, southern Nevada and northwestern Arizona [M.S. thesis]: Las Vegas, University of Nevada Las Vegas, 309 p.

Hay, W.W., and Leslie, M.A., 1990, Could possible changes in global groundwater reservoir cause eustatic sea level fluctuations?, *in* Geophysics Study Committee, Commission on Physical Sciences, Mathematics, and Resources, National Research Council, eds., Sea-Level Change (Studies in Geophysics): Washington D.C., National Academy Press, p. 161–170.

Hazzard, J.C., and Mason, J.F., 1936, Middle Cambrian formations of the Providence and Marble mountains, California: Geological Society of America Bulletin, v. 47, p. 229–240, https://doi.org/10.1130/GSAB-47-229.

Hearing, T.W., Harvey, T.H.P., Williams, M., Leng, M.J., Lamb, A.L., Wilby, P.R., Gabbott, S.E., Pohl, A., and Donnadieu, Y., 2018, An early Cambrian greenhouse climate: Science Advances, v. 4, eaar5690, https://doi.org/10.1126/sciadv.aar5690.

Heller, P.L., Komar, P.D., and Pevear, D.R., 1980, Transport process in ooid genesis: Journal of Sedimentary Petrology, v. 50, p. 943–952, https://doi.org/10.1306/212F7B2B-2B24-11D7-8648000102C1865D.

Hill, J., Tetzlaff, D., Curtis, A., and Wood, R., 2009, Modeling shallow marine carbonate depositional systems: Computers & Geosciences, v. 35, p. 1862–1874, https://doi.org/10.1016/j.cageo.2008.12.006.

Hill, J., Wood, R., Curtis, A., and Tetzlaff, D.M., 2012, Preservation of forcing signals in shallow water carbonate sediments: Sedimentary Geology, v. 275–276, p. 79–92, https://doi.org/10.1016/j.sedgeo.2012.07.017.

Howley, R.A., and Jiang, G.Q., 2010, The Cambrian Drumian carbon isotope excursion (DICE) in the Great Basin, western United States: Palaeogeography, Palaeoclimatology, Palaeoecology, v. 296, p. 138–150, https://doi.org/10.1016/j.palaeo.2010.07.001.

Karlstrom, K., Hagadorn, J., Gehrels, G., Matthews, W., Schmitz, M., Madronich, L., Mulder, J., Pecha, M., Giesler, D., and Crossey, L., 2018, Cambrian Sauk transgression in the Grand Canyon region redefined by detrital zircons: Nature Geoscience, v. 11, p. 438–443, https://doi.org/10.1038/s41561-018-0131-7.

Karlstrom, K.E., Mohr, M.T., Schmitz, M.D., Sundberg, F.A., Rowland, S.M., Blakey, R., Foster, J.R., Crossey, L.J., Dehler, C.M., and Hagadorn, J.W., 2020, Redefining the Tonto Group of Grand Canyon and recalibrating the Cambrian time scale: Geology, v. 48, p. 425–430, https://doi.org/10.1130/G46755.1.

Keller, M., Lehnert, O., and Cooper, J.D., 2012, Sauk megasequence supersequences, southern Great Basin: Second-order accommodation events on the southwestern Cordilleran margin platform, *in* Derby, J., Fritz, R., Longacre, S., Morgan, W., and Sternbach, C., eds., The Great American Carbonate Bank: The Geology and Economic Resources of the Cambrian–Ordovician Sauk Megasequence of Laurentia: American Association of Petroleum Geologists Memoir 98, p. 873–896, https://doi.org/10.1306/13331519M983514.

Kiessling, W., Flügel, E., and Golonka, J., 2003, Patterns of Phanerozoic carbonate platform sedimentation: Lethaia, v. 36, p. 195–225, https://doi.org/10.1080/00241160310004648.

Korolev, V.S., 1997, Sequence stratigraphy, sedimentology, and correlation of the undifferentiated Cambrian dolomites of the Grand Canyon and Lake Mead area [M.S. thesis]: Las Vegas, University of Nevada Las Vegas, 178 p.

Landing, E., 2011, No Late Cambrian shoreline ice in Laurentia; Reply to Runkel et al., 2010: GSA Today, v. 21, p. e20, https://doi.org/10.1130/G124Y.1.

Landing, E., Geyer, G., Buchwaldt, R., and Bowring, S.A., 2015, Geochronology of the Cambrian: A precise Middle Cambrian U-Pb zircon date from the German margin of West Gondwana: Geological Magazine, v. 152, p. 28–40, https://doi.org/10.1017/S0016756814000119.

Lee, Y.I., and Kim, J.C., 1992, Storm-influenced siliciclastic and carbonate ramp deposits, the Lower Ordovician Dumugol Formation, South Korea: Sedimentology, v. 39, p. 951–969, https://doi.org/10.1111/j.1365-3091.1992.tb01990.x.

Lehrmann, D.J., and Goldhammer, R.K., 1999, Secular variation in parasequence and facies stacking patterns of platform carbonates: A guide to application of stacking-patterns analysis in strata of diverse ages and settings, *in* Harris, P.M., Saller, A.H., and Simo, J.A., eds., Advances in Carbonate Sequence Stratigraphy: Application to Reservoirs, Outcrops and Models: SEPM (Society for Sedimentary Geology) Special Publication 63, p. 187–225, https://doi.org/10.2110/pec.99.11.0187.

Levy, M., and Christie-Blick, N., 1989, Pre-Mesozoic palinspastic reconstruction of the eastern Great Basin (western United States): Science, v. 245, p. 1454–1462, https://doi.org/10.1126/science.245.4925.1454.

Lin, J.P., Sundberg, F.A., Jiang, G.Q., Montañez, I.P., and Wotte, T., 2019, Chemostratigraphic correlations across the first major trilobite extinction and faunal turnovers between Laurentia and China: Scientific Reports, v. 9, 17392, https://doi.org/10.1038/s41598-019-53685-2.

Longwell, C.R., 1974, Measure and date of movement on Las Vegas Valley shear zone, Clark County, Nevada: Geological Society of America Bulletin, v. 85, p. 985–990, https://doi.org/10.1130/0016-7606(1974)85<985:MADOMO>2.0.CO;2.

Longwell, C.R., Pampeyan, E.H., Bower, B., and Roberts, R.J., 1965, Geology and mineral deposits of Clark County, Nevada: Nevada Bureau of Mines and Geology Bulletin 62, 218 p.

Matthews, W., Guest, B., and Madronich, L., 2018, Latest Neoproterozoic to Cambrian detrital zircon facies in western Laurentia: Geosphere, v. 14, p. 243–264, https://doi.org/10.1130/GES01544.1.

Matti, J.C., Castor, S.B., Bell, J.W., and Rowland, S.M., 1993, Geologic map of the Las Vegas NE quadrangle: Nevada Bureau of Mines and Geology Map 3Cg, scale 1:24,000.

Mayer, L., and Dickinson, W.R., 1984, Time-thickness bar diagrams: Simultaneous display of lithostratigraphic thickness and chronostratigraphic range: Geology, v. 12, p. 7, https://doi.org/10.1130/0091-7613(1984)12<7:TBDSDO>2.0.CO;2.

McKee, E.D., 1945, Stratigraphy and ecology of the Grand Canyon Cambrian, *in* McKee, E.D., and Resser, C.E., Cambrian History of the Grand Canyon Region: Carnegie Institution of Washington Publication 563, Part I, p. 3–168.

Meng, X.H., Ge, M., and Tucker, M.E., 1997, Sequence stratigraphy, sea-level changes and depositional systems in the Cambro-Ordovician of the North China carbonate platform: Sedimentary Geology, v. 114, p. 189–222, https://doi.org/10.1016/S0037-0738(97)00073-0.

Middleton, L.T., and Elliott, D.K., 2003, Tonto Group, *in* Beus, S.S., and Morales, M., eds., Grand Canyon Geology (2nd edition): New York, Oxford University Press, p. 90–114.

Miller, R.H., and Zilinsky, G.A., 1981, Lower Ordovician through Lower Devonian cratonic margin rocks of the southern Great Basin: Geological Society of America Bulletin, v. 92, p. 255–261, https://doi.org/10.1130/0016-7606(1981)92<255:LOTLDC>2.0.CO;2.

Miller, R.H., Cooper, J.D., and Sundberg, F.A., 1981, Upper Cambrian faunal distribution in southeastern California and southern Nevada, *in* Taylor, M.E., ed., Short Papers for the Second International Symposium on the Cambrian System: U.S. Geological Survey Open-File Report 81-743, p. 138–142, https://doi.org/10.3133/ofr81743.

Montañez, I.P., and Osleger, D.A., 1993, Parasequence stacking patterns, third-order accommodation events, and sequence stratigraphy of Middle to Upper Cambrian platform carbonates, Bonanza King Formation, southern Great Basin, *in* Loucks, R.G., and Sarg, J.F., eds., Carbonate Sequence Stratigraphy: Recent Developments and Applications: American Association of Petroleum Geologists Memoir 57, p. 305–326, https://doi.org/10.1306/M57579C12.

Montañez, I.P., Osleger, D.A., Banner, J.L., Mack, L.E., and Musgrove, M., 2000, Evolution of the Sr and C isotope composition of Cambrian oceans: GSA Today, v. 10, no. 5, p. 1–7.

Morgan, W.A., 2012, Sequence stratigraphy of the Great American Carbonate Bank, *in* Derby, J., Fritz, R., Longacre, S., Morgan, W., and Sternbach, C., eds., The Great American Carbonate Bank: The Geology and Economic Resources of the Cambrian–Ordovician Sauk Megasequence of Laurentia: American Association of Petroleum Geologists Memoir 98, p. 37–82, https://doi.org/10.1306/13331489M981333.

Myrow, P.M., Tice, L., Archuleta, B., Clark, B., Taylor, J.F., and Ripperdan, R.L., 2004, Flat-pebble conglomerate: Its multiple origins and relationship to metre-scale depositional cycles: Sedimentology, v. 51, p. 973–996, https://doi.org/10.1111/j.1365-3091.2004.00657.x.

Noble, L.F., 1914, The Shinumo quadrangle, Grand Canyon district, Arizona: U.S. Geological Survey Bulletin 549, 154 p., https://doi.org/10.3133/b549.

Noble, L.F., 1922, A section of the Paleozoic formations of the Grand Canyon at Bass Trail: U.S. Geological Survey Professional Paper 131-B, 50 p., https://doi.org/10.3133/pp131B.

Noffke, N., and Awramik, S.M., 2013, Stromatolites and MISS—Differences between relatives: GSA Today, v. 23, no. 9, p. 4–9, https://doi.org/10.1130/GSATG187A.1.

North American Commission on Stratigraphic Nomenclature, 2005, North American Stratigraphic Code: American Association of Petroleum Geologists Bulletin, v. 89, p. 1547–1591, https://doi.org/10.1306/07050504129.

Osleger, D.A., and Montañez, I.P., 1996, Cross-platform architecture of a sequence boundary in mixed siliciclastic-carbonate lithofacies, Middle Cambrian, southern Great Basin, USA: Sedimentology, v. 43, p. 197–217, https://doi.org/10.1046/j.1365-3091.1996.d01-13.x.

Osleger, D.A., and Read, J.F., 1991, Relation of eustasy to stacking patterns of meter-scale carbonate cycles, Late Cambrian, U.S.A.: Journal of Sedimentary Petrology, v. 61,

p. 1225–1252, https://doi.org/10.1306/D426786B-2B26-11D7-8648000102C1865D.

Osleger, D.A., Montañez, I.P., Martin-Chivelet, J., and Lehmann, C., 1996, Cycle and sequence stratigraphy of Middle to Upper Cambrian carbonates, Bonanza King Formation, southern Great Basin, *in* Abbott, P.L., and Cooper, J.D., eds., Field Conference Guidebook and Volume for the American Association of Petroleum Geologists Annual Convention, San Diego, California, May 1996: Pacific Section American Association of Petroleum Geologists Guidebook 73, p. 55–84, https://doi.org/10.32375/1996-GB73.5.

Pack, P.D., and Gayle, H.B., 1971, A new olenellid trilobite, *Bieratops nevadensis*, from the Lower Cambrian near Las Vegas, Nevada: Journal of Paleontology, v. 45, p. 893–898.

Page, W.R., Lundstrom, S.C., Harris, A.G., Langenheim, V.E., Workman, J.B., Mahan, S.A., Paces, J.B., Dixon, G.L., Rowley, P.D., Burchfield, B.C., Bell, J.W., and Smith, E.I., 2004, Geologic and geophysical maps of the Las Vegas 30′ × 60′ quadrangle, Clark and Nye counties, Nevada, and Inyo County, California: U.S. Geological Survey Scientific Investigations Map 2814, scale 1:5,000,000, https://doi.org/10.3133/sim2814.

Palmer, A.R., 1979, Biomere boundaries re-examined: Alcheringa, v. 3, p. 33–41, https://doi.org/10.1080/03115517908565438.

Palmer, A.R., and Halley, R.B., 1979, Physical stratigraphy and trilobite biostratigraphy of the Carrara Formation (Lower and Middle Cambrian) in the southern Great Basin: U.S. Geological Survey Professional Paper 1047, 131 p., https://doi.org/10.3133/pp1047.

Palmer, A.R., and Hazzard, J.C., 1956, Age and correlation of Cornfield Springs and Bonanza King formations in southeastern California and southern Nevada: American Association of Petroleum Geologists Bulletin, v. 40, p. 2494–2499, https://doi.org/10.1306/5CEAE5AA-16BB-11D7-8645000102C1865D.

Peng, S.C., Babcock, L.E., and Cooper, R.A., 2012, The Cambrian Period, *in* Gradstein, F.M., Ogg, J.G., Schmitz, M.D., and Ogg, G.M., eds., The Geologic Time Scale 2012: Amsterdam, Elsevier, p. 437–488, https://doi.org/10.1016/B978-0-444-59425-9.00019-6.

Peng, S.C., Babcock, L.E., and Ahlberg, P., 2020, The Cambrian Period, *in* Gradstein, F.M., Ogg, J.G., Schmitz, M.D., and Ogg, G.M., eds., The Geologic Time Scale 2020: Amsterdam, Elsevier, p. 565–629, https://doi.org/10.1016/B978-0-12-824360-2.00019-X.

Peters, S.E., and Gaines, R.R., 2012, Formation of the 'Great Unconformity' as a trigger for the Cambrian explosion: Nature, v. 484, p. 363–366, https://doi.org/10.1038/nature10969.

Powell, J.W., 1876, Report on the geology of the eastern portion of the Uinta Mountains and a region of country adjacent thereto: Washington, D.C., U.S. Geological and Geographical Survey of the Territories, 218 p., https://doi.org/10.3133/70039913.

Pratt, B.R., and James, N.P., 1986, The St. George Group (Lower Ordovician) of western Newfoundland: Tidal flat island model for carbonate sedimentation in shallow epeiric seas: Sedimentology, v. 33, p. 313–343, https://doi.org/10.1111/j.1365-3091.1986.tb00540.x.

Pratt, B.R., and Rule, R.G., 2021, A Mesoproterozoic carbonate platform (lower Belt Supergroup of western North America): Sediments, facies, tides, tsunamis and earthquakes in a tectonically active intracratonic basin: Earth-Science Reviews, v. 217, 103626, https://doi.org/10.1016/j.earscirev.2021.103626.

Pulsipher, M.A., Schiffbauer, J.D., Jeffrey, M.J., Huntley, J.W., Fike, D.A., and Shelton, K.L., 2021, A meta-analysis of the Steptoean Positive Carbon Isotope Excursion: The SPICEraq database: Earth-Science Reviews, v. 212, https://doi.org/10.1016/j.earscirev.2020.103442.

Purkis, S.J., Rowlands, G.P., and Kerr, J.M., 2015, Unravelling the influence of water depth and wave energy on the facies diversity of shelf carbonates: Sedimentology, v. 62, p. 541–565, https://doi.org/10.1111/sed.12110.

Rankey, E.C., 2004, On the interpretation of shallow shelf carbonate facies and habitats: How much does water depth matter?: Journal of Sedimentary Research, v. 74, p. 2–6, https://doi.org/10.1306/071803740002.

Resser, C.E., 1945, Cambrian fossils of the Grand Canyon, *in* McKee, E.D., and Resser, C.E., Cambrian History of the Grand Canyon Region: Carnegie Institution of Washington Publication 563, Part II, p. 169–220.

Robison, R.A., 1965, Middle Cambrian eocrinoids from western North America: Journal of Paleontology, v. 39, p. 355–364.

Rose, E.C., 2003, Depositional environment and history of the Cambrian Tonto Group, Grand Canyon, Arizona [M.S. thesis]: Flagstaff, Northern Arizona University, 349 p.

Rose, E.C., 2006, Nonmarine aspects of the Tonto Group of the Grand Canyon, USA, and broader implications: Palaeoworld, v. 15, p. 223–241, https://doi.org/10.1016/j.palwor.2006.10.008.

Rose, E.C., 2011, Modification of the nomenclature and a revised depositional model for the Cambrian Tonto Group of the Grand Canyon, Arizona, *in* Hollingsworth, J.S., Sundberg, F.A., and Foster, J.R., eds., Cambrian Stratigraphy and Paleontology of Northern Arizona and Southern Nevada: Museum of Northern Arizona Bulletin 67, p. 77–98.

Rowland, S.M., 1987, Paleozoic stratigraphy of Frenchman Mountain, Clark County, Nevada, *in* Hill, M.L., ed., Cordilleran Section of the Geological Society of America: Geological Society of America Centennial Field Guide 1, p. 53–56, https://doi.org/10.1130/0-8137-5401-1.53.

Rowland, S.M., 2022, Geology of Frenchman Mountain and Rainbow Gardens, southern Nevada, USA, *in* Jiang, G.Q., and Dehler, C., eds., Field Excursions from Las Vegas, Nevada: Guides to the 2022 GSA Cordilleran and Rocky Mountain Joint Section Meeting: Geological Society of America Field Guide 63, p. 23–43, https://doi.org/10.1130/2022.0063(02).

Rowland, S.M., and Korolev, S.S., 2011, How old is the top of the Tonto Group in Grand Canyon, *in* Hollingsworth, J.S., Sundberg, F.A., and Foster, J.R., eds., Cambrian Stratigraphy and Paleontology of Northern Arizona and Southern Nevada: Museum of Northern Arizona Bulletin 67, p. 304.

Rowland, S.M., and Shapiro, R.S., 2002, Reef patterns and environmental influences in the Cambrian and earliest Ordovician, *in* Kiessling, W., Flügel, E., and Golonka, J., eds., Phanerozoic Reef Patterns: SEPM (Society for Sedimentary Geology) Special Publication 72, p. 95–128, https://doi.org/10.2110/pec.02.72.0095.

Rowland, S.M., Parolini, J.R., Eschner, E., McAllister, A.J., and Rice, J.A., 1990, Sedimentologic and stratigraphic constraints on the Neogene translation and rotation of the Frenchman Mountain structural block, Clark County, Nevada, *in* Wernicke, B.P., ed., Basin and Range Extensional Tectonics near the Latitude of Las Vegas, Nevada: Geological Society of America Memoir 176, p. 99–122, https://doi.org/10.1130/MEM176-p99.

Rowland, S.M., Osborn, G.D., and Graber, D.J., 1995, Lower Paleozoic stratigraphy of Fern Glen Canyon, Central Grand Canyon: Journal of the Arizona-Nevada Academy of Science, v. 28, p. 1–11.

Runkel, A.C., Mackey, T.J., Cowan, C.A., and Fox, D.L., 2010, Tropical shoreline ice in the late Cambrian: Implications for Earth's climate between the Cambrian explosion and the Great Ordovician biodiversification event: GSA Today, v. 20, p. 4–10, https://doi.org/10.1130/GSATG84A.1.

Saltzman, M.R., Runnegar, B., and Lohmann, K.C., 1998, Carbon isotope stratigraphy of Upper Cambrian (Steptoean Stage) sequences of the eastern Great Basin: Record of a global oceanographic event: Geological Society of America Bulletin, v. 110, p. 285–297, https://doi.org/10.1130/0016-7606(1998)110<0285:CISOUC>2.3.CO;2.

Saltzman, M.R., Brasier, M.D., Ripperdan, R.L., Ergaliev, G.K., Lohman, K.C., Robison, R.A., Chang, W.T., Peng, S.C., and Runnegar, B., 2000, A global carbon isotope excursion during the Late Cambrian: Relation to trilobite extinction, organic-matter burial and sea level: Palaeogeography, Palaeoclimatology, Palaeoecology, v. 162, p. 211–223, https://doi.org/10.1016/S0031-0182(00)00128-0.

Saltzman, M.R., Cowan, C.A., Runkel, A.C., Runnegar, B., Stewart, M.C., and Palmer, A.R., 2004, The Late Cambrian SPICE ($\delta^{13}C$) event and the Sauk II–Sauk III regression: New evidence from Laurentian basins in Utah, Iowa, and Newfoundland: Journal of Sedimentary Research, v. 74, p. 366–377, https://doi.org/10.1306/120203740366.

Sames, B., Wagreich, M., Conrad, C.P., and Iqbal, S., 2020, Aquifer-eustasy as the main driver of short-term sea-level fluctuations during Cretaceous hothouse climate phases, *in* Wagreich, M., Hart, M., Sames, B., and Yilmaz, I.O., eds., Cretaceous Climate Events and Short-Term Sea-Level Changes: Geological Society of London Special Publication 498, p. 9–38, https://doi.org/10.1144/SP498-2019-105.

Schenk, E.T., and Wheeler, H.E., 1942, Cambrian sequence in western Grand Canyon, Arizona: The Journal of Geology, v. 50, p. 882–899, https://doi.org/10.1086/625089.

Schiffbauer, J.D., Huntley, J.W., Fike, D.A., Jeffrey, M.J., Gregg, J.M., and Shelton, K.L., 2017, Decoupling biogeochemical records, extinction, and environmental change during the Cambrian SPICE event: Science Advances, v. 3, https://doi.org/10.1126/sciadv.1602158.

Schwab, F.L., 1976, Modern and ancient sedimentary basins: Comparative accumulation rates: Geology, v. 4, p. 723–727, https://doi.org/10.1130/0091-7613(1976)4<723:MAASBC>2.0.CO;2.

Shapiro, R.S., and Awramik, S.M., 2000, Microbialite morphostratigraphy as a tool for correlating Late Cambrian and Early Ordovician sequences: The Journal of Geology, v. 108, p. 171–180, https://doi.org/10.1086/314394.

Shembilu, N., and Azmy, K., 2021, Carbon-isotope stratigraphy of the Middle–Upper Cambrian of eastern Laurentia: Implications for global correlation: Marine and Petroleum Geology, v. 128, https://doi.org/10.1016/j.marpetgeo.2021.105052.

Shinn, E.A., 1983, Tidal flat environment, *in* Scholle, P.A., Bebout, D.G., and Moore, C.H., eds., Carbonate Depositional Environments: American Association of Petroleum Geologists Memoir 33, p. 171–210, https://doi.org/10.1306/M33429C8.

Sprinkle, J., and Kier, P.M., 1987, Phylum Echinodermata, *in* Boardman, R.S., Cheetham, A.H., and Rowell, A.J., eds.,

Fossil Invertebrates: Palo Alto, California, Blackwell Scientific, p. 550–611.
Stephens, G.L., Kahn, B.H., and Richardson, M., 2016, The super greenhouse effect in a changing climate: Journal of Climate, v. 29, p. 5469–5482, https://doi.org/10.1175/JCLI-D-15-0234.1.
Strasser, A., 2015, Hiatuses and condensation: An estimation of time lost on a shallow carbonate platform: The Depositional Record, v. 1, p. 91–117, https://doi.org/10.1002/dep2.9.
Sundberg, F.A., 1979, Upper Cambrian paleobiology and depositional environments of the lower Nopah Formation, California and Nevada [M.S. thesis]: San Diego, California, San Diego State University, 183 p.
Sundberg, F.A., 1991, Paleogeography of western Utah and eastern Nevada during the *Ehmaniella* Biochron (Middle Cambrian), *in* Cooper, J.D., and Stevens, C.H., eds., Paleozoic Paleogeography of the Western United States—II: Los Angeles, Pacific Section SEPM (Society for Sedimentary Geology), p. 387–399.
Sundberg, F.A., 2011, Stop 3: Cambrian of Peach Springs Canyon, Hualapai Indian Reservation, Arizona, *in* Hollingsworth, J.S., Sundberg, F.A., and Foster, J.R., eds., Cambrian Stratigraphy and Paleontology of Northern Arizona and Southern Nevada: Museum of Northern Arizona Bulletin 67, p. 186–191.
Sundberg, F.A., McCollum, L.B., and McCollum, M.B., 2011, Stop 7C: Stratigraphy of the Laurentian uppermost Dyeran Stage to Skullrockian Stage, Emigrant Formation at Split Mountain, Esmeralda County, Nevada, *in* Hollingsworth, J.S., Sundberg, F.A., and Foster, J.R., eds., Cambrian Stratigraphy and Paleontology of Northern Arizona and Southern Nevada: Museum of Northern Arizona Bulletin 67, p. 246–252.
Sundberg, F.A., Karlstrom, K.E., Geyer, G., Foster, J.R., Hagadorn, J.W., Mohr, M.T., Schmitz, M.D., Dehler, C.M., and Crossey, L.J., 2020, Asynchronous trilobite extinctions at the early to middle Cambrian transition: Geology, v. 48, p. 441–445, https://doi.org/10.1130/G46913.1.
Taylor, J.F., Repetski, J.E., Loch, J.D., and Leslie, S.A., 2012, Biostratigraphy and chronostratigraphy of the Cambrian–Ordovician great American carbonate bank, *in* Derby, J.R., Fritz, R.D., Longacre, S.A., Morgan, W.A., and Sternbach, C.A., eds., The Great American Carbonate Bank: The Geology and Economic Resources of the Cambrian–Ordovician Sauk Megasequence of Laurentia: American Association of Petroleum Geologists Memoir 98, p. 15–35, https://doi.org/10.1306/13331488M983497.
Torsvik, T.H., and Cocks, L.R.M., 2017, Earth History and Palaeogeography: Cambridge, UK, Cambridge University Press, 317 p.
Webster, M., 2011a, Trilobite biostratigraphy and sequence stratigraphy of the upper Dyeran (traditional Laurentian "Lower Cambrian") in the southern Great Basin, U.S.A., *in* Hollingsworth, J.S., Sundberg, F.A., and Foster, J.R., eds., Cambrian Stratigraphy and Paleontology of Northern Arizona and Southern Nevada: Museum of Northern Arizona Bulletin 67, p. 121–154.
Webster, M., 2011b, Stop 4B: Litho- and biostratigraphy of the Dyeran-Delamaran boundary interval at Frenchman Mountain, Nevada, *in* Hollingsworth, J.S., Sundberg, F.A., and Foster, J.R., eds., Cambrian Stratigraphy and Paleontology of Northern Arizona and Southern Nevada: Museum of Northern Arizona Bulletin 67, p. 195–203.
Webster, M., 2011c, Stops 7A, 7B, and 7C: Upper Dyeran litho- and biostratigraphy of the Split Mountain area, Nevada, *in* Hollingsworth, J.S., Sundberg, F.A., and Foster, J.R., eds., Cambrian Stratigraphy and Paleontology of Northern Arizona and Southern Nevada: Museum of Northern Arizona Bulletin 67, p. 236–246.
Webster, M., McCollum, L.B., and Sundberg, F.A., 2011, Stop 6B: Upper Dyeran and lower Delamaran lithostratigraphy and biostratigraphy of the northern Groom Range, Nevada, *in* Hollingsworth, J.S., Sundberg, F.A., and Foster, J.R., eds., Cambrian Stratigraphy and Paleontology of Northern Arizona and Southern Nevada: Museum of Northern Arizona Bulletin 67, p. 226–236.
Wendler, J.E., and Wendler, I., 2016, What drove sea-level fluctuations during the mid-Cretaceous greenhouse climate?: Palaeogeography, Palaeoclimatology, Palaeoecology, v. 441, p. 412–419, https://doi.org/10.1016/j.palaeo.2015.08.029.
Wendler, J.E., Wendler, I., Vogt, C., and Kuss, J., 2016, Link between cyclic eustatic sea-level change and continental weathering: Evidence for aquifer-eustasy in the Cretaceous: Palaeogeography, Palaeoclimatology, Palaeoecology, v. 441, p. 430–437, https://doi.org/10.1016/j.palaeo.2015.08.014.
Wernicke, B., Axen, G.J., and Snow, J.K., 1988, Basin and Range extensional tectonics at the latitude of Las Vegas, Nevada: Geological Society of America Bulletin, v. 100, p. 1738–1757, https://doi.org/10.1130/0016-7606(1988)100<1738:BARETA>2.3.CO;2.
Widiarti, R., 2011, Lateral variability of facies and cycles in the Furongian (Late Cambrian) Carbonate Platform: An example from the Big Horse Member of the Orr Formation in western Utah, U.S.A. [M.S. thesis]: Las Vegas, University of Nevada Las Vegas, 58 p.
Wilkinson, B.H., Diedrich, N.W., Drummond, C.N., and Rothman, E.D., 1998, Michigan hockey, meteoric precipitation, and rhythmicity of accumulation on peritidal carbonate platforms: Geological Society of America Bulletin, v. 110, p. 1075–1093, https://doi.org/10.1130/0016-7606(1998)110<1075:MHMPAR>2.3.CO;2.
Wotte, T., Skovsted, C.B., Whitehouse, M.J., and Kouchinsky, A., 2019, Isotopic evidence for temperate oceans during the Cambrian explosion: Scientific Reports, v. 9, 6330, https://doi.org/10.1038/s41598-019-42719-4.
Wright, V.P., and Burchette, H.L., 1996, Shallow-water carbonate environments, *in* Reading, H.G., ed., Sedimentary Environments (3rd edition): Processes, Facies, and Stratigraphy: Malden, Massachusetts, Blackwell Science, p. 325–394.
Zeiza, A.D., 2010, Tectonically controlled autocyclicity in the Furongian (Late Cambrian) carbonate platform, central-Nevada and western Utah, U.S.A. [M.S. thesis]: Las Vegas, University of Nevada Las Vegas, 90 p.
Zhang, Y.Q., Chen, D.Z., Zhou, X.Q., Guo, Z.H., Wei, W.W., and Mutti, M., 2015, Depositional facies and stratal cyclicity of dolomites in the Lower Qiulitag Group (Upper Cambrian) in northwestern Tarim Basin, NW China: Facies, v. 61, 417, https://doi.org/10.1007/s10347-014-0417-1.
Zhu, M.Y., Zhang, J.M., Li, G.X., and Yang, A.H., 2004, Evolution of C isotopes in the Cambrian of China: Implications for Cambrian subdivisions and trilobite mass extinctions: Geobios, v. 37, p. 287–301, https://doi.org/10.1016/j.geobios.2003.06.001.